Received 6 May 2024; revised 12 June 2024; accepted 27 July 2024. Date of publication 2 August 2024; date of current version 16 August 2024.

Digital Object Identifier 10.1109/OJCOMS.2024.3437661

Estimation of the User Position and Orientation in mmWave Cellular Networks Aided by an Active RIS

GEORGIOS MYLONOPOULOS [1,2] (Student Member, IEEE), LUCA VENTURINO [1,2] (Senior Member, IEEE), STEFANO BUZZI [1,2,3] (Senior Member, IEEE), AND CARMEN D'ANDREA [1,2] (Member, IEEE)

[1]Department of Electrical and Information Engineering, University of Cassino and Southern Latium, 03043 Cassino, Italy

[2]Consorzio Nazionale Interuniversitario per le Telecomunicazioni, 43124 Parma, Italy

[3]Dipartimento di Elettronica Informazione e Bioingegneria, Politecnico di Milano, 20133 Milan, Italy

CORRESPONDING AUTHOR: G. MYLONOPOULOS (e-mail: georgios.mylonopoulos@unicas.it)

This work was supported in part by the European Union's Horizon 2020 Research and Innovation Programme under the Marie Sklodowska-Curie Grant under Agreement 956256. The work of Luca Venturino was supported by the European Union – NextGenerationEU – National Recovery and Resilience Plan, Mission 4, Component 2, Investment 1.1, Call PRIN 2022 D.D. 104 02/02/2022 (Project "CIRCE," CUP H53D23000420006) under Grant 202238BJ2R.

ABSTRACT This paper considers an OFDM-based wireless cellular network operating at millimeter waves and studies the problem of estimating the position and orientation of a mobile station (MS) upon relying on the pilot symbols emitted by the serving base station (BS), which are received via a direct link and an indirect link provided by a reconfigurable intelligent surface (RIS). To counterbalance the multiplicative pathloss in the indirect link, an active RIS is employed, which is able to reflect and amplify the incident signal. Upon introducing a convenient signal model, which accounts for the additional noise generated by the reflective amplifiers in the active RIS, we derive the ML estimators of the MS position and orientation and the corresponding Cramér Rao Lower Bounds under three levels of system cognition at the MS concerning the BS beamforming matrix, the RIS response, and the channel amplitudes on the direct and indirect links. In two cases, we also derive a suboptimal estimator with a reduced implementation complexity. Finally, we provide a numerical analysis to show the merits of the proposed estimators, assess the achievable gains granted by the use of an active RIS (as compared to a passive one), and investigate the impact of the main system parameters, including the BS-RIS distance and the amplification gain at the RIS.

INDEX TERMS Active reconfigurable intelligent surfaces, localization, orientation, millimeter waves, maximum likelihood estimation.

I. INTRODUCTION

RECONFIGURABLE Intelligent Surfaces (RISs) are made of metamaterial elements, arranged on a regular grid with sub-wavelength spacing, that are capable of reflecting the impinging radio waves with a tunable phase shift and, in some cases, of amplifying them [1]. The ability to control the propagation channel introduces new degrees of freedom for system design [2], changing the classical communication paradigm, which assumes that only the transmitter and the receiver can be engineered to increase the performance, without the ability to control the channel. From an industrial point of view, RISs appear to be an attractive mean to extend the coverage of a wireless network without deploying a more expensive repeater or a network node [3]. RISs, indeed, may illuminate areas otherwise not visible to the base station (BS). RISs prove to also be useful within covered areas, since they create helpful macro-diversity by providing reliable multipath links [4]. In that sense, properly tuning the phases imposed by the RIS elements on the reflected waves allows to concentrate the signal towards a desired point or direction, thus increasing the signal-to-noise ratio (SNR) in a spatially favorable manner [5].

© 2024 The Authors. This work is licensed under a Creative Commons Attribution-NonCommercial-NoDerivatives 4.0 License.
For more information, see https://creativecommons.org/licenses/by-nc-nd/4.0/

While RISs were initially proposed for communication purposes, they are also helpful for localization [6]. Notable contributions in this area include the studies [7], [8], [9], [10], [11], that explore the core idea of extracting positional information from the indirect links provided by the RISs. In particular, [7] considers a passive RIS for uplink user localization and derives the Cramér-Rao lower bounds (CRLBs) for the estimation of the position and orientation, while proposing several strategies for the RIS design. Similarly, in [8], it is illustrated that accurate localization of mobile stations (MSs) with a single access point is possible due to the RIS ability to mark the channel, compared to random multipath links. In [9], the use of RISs for wireless fingerprinting localization is considered and two solutions (one based on machine learning and one on correlated noise heuristic estimators) are proposed for improving localization accuracy; in particular, the presence of the RISs permits reducing the number of access points. Indoor RIS-aided multi-user localization based on measured received signal strength is considered in [10], where the additional indirect links are utilized for an RIS-aided localization protocol, along with a proposed RIS-design methodology to minimize the probabilities of false localization. Furthermore, the authors in [11] address the RIS-aided localization of a MS with a single BS and propose iterative algorithms to update the RIS configuration to minimize the CRLB on the position estimation error.

Other studies have considered the problem of clock offset estimation, along with the RIS-aided localization, with the corresponding Fisher information analysis [12], [13]. Moreover, when the MS is equipped with multiple antennas, the joint localization and synchronization may include the estimation of the MS orientation (bearing) [14], highlighting that RIS-aided localization may extend to more practical scenarios.

It is also worth noting, that RISs may be useful for target tracking [15], simultaneous localization and mapping procedures [6], simultaneous localization and sensing [16] and radar-like sensing applications [17], [18], [19], [20]. Particularly, with an RIS, multiple targets may be inspected, either with an adaptive feedback channel [17], or via multiple sensing beams, formed by the RIS reflection [18]. The RIS placement relative to the inspected target [19] and the radar transmitter/receiver [20] is fundamental, as it reduces the multiplicative fading along the RIS-provided link. Interestingly, an RIS can also be mounted on a moving vehicle, as shown in [21]; here, the presence of the RIS helps the BS to estimate the position of the vehicle and, at the same, time sustains a communication link with near users. The variety of the considered scenarios highlights the degrees of freedom offered by RISs in spatially aware applications.

The shape, size and structure of RISs are versatile, fit for numerous sensing applications, that need to be investigated. For example, when considering indoor positioning and large RISs, the far-field conditions are not necessarily fulfilled and it is of primary interest to also investigate localization algorithms for the near-field. In [22] an indoor scenario is considered, where the RIS has a planar rectangular structure with one dimension much larger than the other, such that the far-field conditions do not hold. Assuming single anchor node, the paper develops localization algorithms when downlink orthogonal frequency division multiplexing (OFDM) signals are transmitted. Additionally, in [23], an RIS operates as a lens receiver and the localization of a transmitter in close proximity is investigated, taking into account the near-field effects. The impact of different lens configurations on the Fisher information matrix (FIM) is evaluated, and a two-stage localization algorithm is proposed.

All previously referenced papers focus on the usage of a passive RIS. In this context, a major shortcoming of passive RIS is the double pathloss effect, since the overall path is the cascade of two hops, one linking the BS and the RIS and one linking the RIS and the MS [24], which implies that the RIS may be helpful only when placed sufficiently close to the BS or MS. To mitigate this issue, the usage of active RISs has been recently proposed, providing a powerful indirect link, comparable to the direct link [25], [26], [27], [28], [29]. The elements of an active RIS are capable of introducing an amplification to the reflected waves on top of the phase change, alleviating the multiplicative fading phenomenon. Thus, higher SNR [25] and better sum-rate performance [26] are achieved, in terms of communication efficiency, compared to networks enabled with passive RISs. In addition, an active RIS can prove useful in sensing applications, as it provides angular diversity with powerful target illumination [27], mimicking the multi-static distributed radar, without the cost of additional radio frequency (RF) chains [28]. The merits of active RISs for MS localization have been also very recently highlighted in [30], wherein an approach based on neural networks is proposed to estimate at a RIS-aided BS the position of an MS transmitting a known pilot sequence.

The amplification granted by active RISs may be obtained through integrated reflection-type amplifiers, which can be built using current-inverting converters [31], integrated circuits [32], or asymmetric current mirrors [33]. An active RIS can be built either with all of its reflective elements being active [34] -which can even support nonreciprocal, full duplex amplification- or by partially distributing active elements among passive elements, either with a fixed or a dynamic architecture [35], generating additional degrees of freedom in the deployment problem, i.e., allocating the active RIS elements among the passive ones. It needs to be clarified, that active RISs do not entail any signal processing capabilities, since their elements are based on an electronic circuit that simply amplifies and superimposes a phase shift on the impinging waves.

More complex RIS structures have also been investigated to allow more elaborate communication procedures and sensing techniques. In [36], the considered RIS is enriched with an RF chain for baseband measurements and signal processing capabilities, thus supporting explicit estimation

of the RIS-aided channel. A semi-passive RIS equipped with dedicated receiving sensors is considered in [37]: here, the RIS redirects a sensing signal transmitted by the BS towards a region otherwise blocked and receives the echos of prospective targets. A similar architecture is considered in [38].

To the best of our knowledge, this paper is the first comprehensive study investigating the usefulness of active -amplify and reflect- RISs for MS localization and orientation estimation, building upon the preliminary studies in [39], [40]. It is worth underlining that we deal with the problem of active localization, i.e., the MS, based on suitable downlink signals transmitted by the BS, estimates its position and orientation; the problem of localizing and/or detection the possible presence of a non-cooperating MS/target is not addressed here. We explore the localization problem in an OFDM-based millimeter wave (mmWave) system aided with an active RIS where a single BS serves a MS without any line-of-sight obstructions. Within this framework, the RIS amplification provides an additional -sufficiently powerful- link, overcoming the multiplicative fading shortcomings of passive RISs. The localization procedure refers to the MS estimating its own position and antenna array orientation, utilizing a known pilot sequence, transmitted by the BS, through optimal and suboptimal solutions, under different design assumptions. The considered scenarios and the proposed estimators pose a trade-off in terms of estimation accuracy, computational complexity, and prior signaling overhead requirements. The major contributions of this paper are summarized in the following.

- A detailed system model is introduced. The considered model takes into account the power amplification at the active RIS acting as an additional noise source; the mathematical analysis is distinctively different from the one commonly found for passive RIS systems.
- The maximum-likelihood (ML) estimators for the position and the array orientation of the MS are derived under three levels of a priori knowledge available at the MS concerning the BS beamforming matrix, the RIS response, and the channel amplitudes on the direct and indirect links. In two cases, a suboptimal estimator with a reduced implementation complexity is also derived.
- For all the three considered cases of prior cognition available at the MS, a lower bound to the achievable performance, in the form of CRLB, is analytically derived. The presence of the dynamic noise introduced by the active RIS makes the procedure for CRLB computation significantly different from that usually followed for passive RISs.
- Extensive numerical results are shown and discussed, to explore the performance of the proposed estimators, also in comparison w.r.t. the derived CRLBs, and investigate the impact of the main system parameters, including the RIS placement, on the achievable estimation performance.

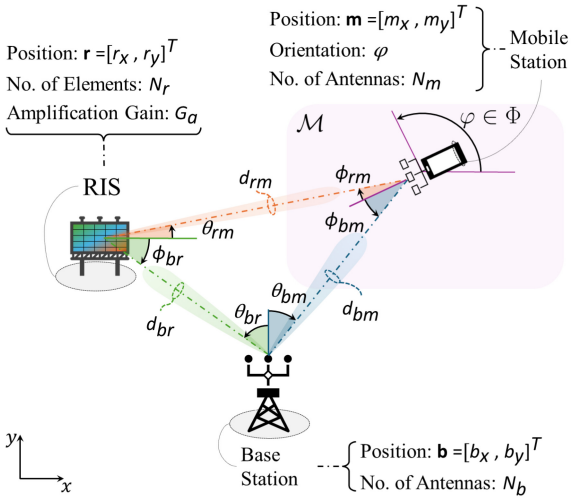

FIGURE 1. Considered system geometry. The BS, located at b, transmits Q pilot sequences towards the RIS, located at r, and the region $\mathcal{M}$. The MS, located at $m \in \mathcal{M}$, receives the pilot symbols directly and via the RIS reflection.

The remainder of this paper is organized as follows. Sec. II contains the system description. Sec. III provides the derivations of the proposed estimators. Sec. IV contains the CRLBs on the estimation of the MS position and orientation and the numerical analysis. Concluding remarks are given in Sec. V, while the Appendix contains analytical derivations.

Notation: Vectors (matrices) are denoted by lowercase (uppercase) boldface letters. $(\cdot)^*$, $(\cdot)^T$, and $(\cdot)^H$ denote conjugate, transpose, and conjugate-transpose, respectively. $\boldsymbol{I}_M$ is the $M \times M$ identity matrix. $\|\boldsymbol{\alpha}\|$ and $[\boldsymbol{\alpha}]_n$ are the Euclidean norm and the n-th entry of the vector $\boldsymbol{\alpha}$. vec$\{\boldsymbol{A}\}$ is the MN dimensional vector obtained by concatenating the columns of the $M \times N$ matrix $\boldsymbol{A}$. diag$\{\boldsymbol{\alpha}\}$ is the $N \times N$ diagonal matrix with the entries of the N-dimensional vector $\boldsymbol{\alpha}$. rank$\{\boldsymbol{A}\}$ and $\boldsymbol{A}^+$ are the rank and the pseudoinverse of the matrix $\boldsymbol{A}$. tr$\{\boldsymbol{A}\}$ and det$\{\boldsymbol{A}\}$ are the trace and the determinant of the square matrix $\boldsymbol{A}$. Finally, $\otimes$ and i denote the Kronecker product and the imaginary unit.

II. SYSTEM DESCRIPTION

We consider the system in Fig. 1, wherein a MS aims to self-estimate its position and orientation upon exploiting the downlink pilot symbols emitted by a near BS assisted by an active RIS. For illustration, we consider a two-dimensional geometry to keep the notation concealed; however, the system description and the following developments can readily be extended to a three-dimensional geometry.[1]

We denote by $\boldsymbol{b} = [b_x, b_y]^T$, $\boldsymbol{r} = [r_x, r_y]^T$ and $\boldsymbol{m} = [m_x, m_y]^T$ the coordinate vectors of the BS, RIS, and MS, respectively; also, we denote by φ the angle specifying the orientation of the array of the MS. The locations of the BS and RIS are known to the MS; also, the BS and MS are

[1] In a three-dimensional geometry, the position of the MS would be specified by three coordinates, while its orientation by three angles (pitch, yaw, and roll), as discussed in [41].

synchronized. We assume that $\boldsymbol{m} \in \mathcal{M}$ and $\varphi \in \Phi$, where $\mathcal{M} \subset \mathbb{R}^2$ and $\Phi \subset (\pi/2, \pi)$ account for the prior uncertainty as to the MS position and orientation, respectively. The BS and MS are equipped with a uniform linear array containing N_b and N_m isotropic antennas spaced of δ_b and δ_m, respectively, while the RIS has N_r^2 elements arranged into a uniform square array spaced of δ_r along each axis. The BS, RIS, and MS are in each other's far-field, i.e., we have [42]

$$\|\boldsymbol{b}-\boldsymbol{r}\|^2 \geq \max\left\{\frac{2(N_b-1)^2\delta_b^2}{\lambda_o}, \frac{4(N_r-1)^2\delta_r^2}{\lambda_o}\right\}, \quad (1a)$$

$$\|\boldsymbol{b}-\boldsymbol{m}\|^2 \geq \max\left\{\frac{2(N_b-1)^2\delta_b^2}{\lambda_o}, \frac{2(N_m-1)^2\delta_m^2}{\lambda_o}\right\}, \quad (1b)$$

$$\|\boldsymbol{r}-\boldsymbol{m}\|^2 \geq \max\left\{\frac{4(N_r-1)^2\delta_r^2}{\lambda_o}, \frac{2(N_r-1)^2\delta_r^2}{\lambda_o}\right\}, \quad (1c)$$

where $\lambda_o = c/f_o$ and c is the speed of the light.[2]

The BS operates at mmWave and employs an OFDM transmission format with carrier frequency f_o and bandwidth W_o. We assume that $1/W_o \gg \tau_{\max}$, where $\tau_{\max}$ is the largest propagation delay along the BS-MS and BS-RIS-MS paths. We employ a subset of K uniformly-spaced subcarriers and denote by W the corresponding spacing, with W being an integer multiple of W_o. K and W are design parameters, and we assume that $KW \ll f_o$, so that the variation of the steering vectors and of the pathloss across subcarriers can be neglected. Finally, we assume line-of-sight propagation with a free-space pathloss model.

For future reference, we denote by $\boldsymbol{\alpha}_b(\theta) \in \mathbb{C}^{N_b}$, $\boldsymbol{\alpha}_m(\theta) \in \mathbb{C}^{N_m}$, and $\bar{\boldsymbol{\alpha}}_r(\theta) = \mathbf{1}_{N_r} \otimes \boldsymbol{\alpha}_r(\theta) \in \mathbb{C}^{N_r^2}$ the steering vectors of the BS, MS, and RIS towards the direction θ, respectively, where

$$[\boldsymbol{\alpha}_b(\theta)]_n = \mathrm{e}^{-\mathrm{i}\frac{2\pi\delta_b}{\lambda_o}(n-1)\sin(\theta)}, \quad n=1,\dots,N_b, \quad (2a)$$

$$[\boldsymbol{\alpha}_m(\theta)]_n = \mathrm{e}^{-\mathrm{i}\frac{2\pi\delta_m}{\lambda_o}(n-1)\sin(\theta)}, \quad n=1,\dots,N_m, \quad (2b)$$

$$[\boldsymbol{\alpha}_r(\theta)]_n = \mathrm{e}^{-\mathrm{i}\frac{2\pi\delta_r}{\lambda_o}(n-1)\sin(\theta)}, \quad n=1,\dots,N_r. \quad (2c)$$

The times of flight (TOFs) along the BS-MS, BS-RIS, and RIS-MS hops are given by

$$\tau_{bm} = \frac{\|\boldsymbol{b}-\boldsymbol{m}\|}{c}, \quad (3a)$$

$$\tau_{br} = \frac{\|\boldsymbol{b}-\boldsymbol{r}\|}{c}, \quad (3b)$$

$$\tau_{rm} = \frac{\|\boldsymbol{r}-\boldsymbol{m}\|}{c}, \quad (3c)$$

respectively; also, for each hop, the corresponding angles of departure (AODs) are

$$\theta_{bm} = \arcsin((b_x-m_x)/\|\boldsymbol{b}-\boldsymbol{m}\|), \quad (4a)$$

$$\theta_{br} = \arcsin((b_x-r_x)/\|\boldsymbol{b}-\boldsymbol{r}\|), \quad (4b)$$

$$\theta_{rm} = \arcsin\big((m_y-r_y)/\|\boldsymbol{r}-\boldsymbol{m}\|\big), \quad (4c)$$

the corresponding angles of arrival (AOAs) are[3]

$$\phi_{bm} = \theta_{bm} + \pi - \varphi, \quad (5a)$$

$$\phi_{br} = \theta_{br} - \pi/2, \quad (5b)$$

$$\phi_{rm} = \theta_{rm} + \pi/2 - \varphi, \quad (5c)$$

and the corresponding channel amplitudes are

$$\rho_{bm} = \frac{\lambda_o}{4\pi\|\boldsymbol{b}-\boldsymbol{m}\|}, \quad (6a)$$

$$\rho_{br} = \frac{\lambda_o}{4\pi\|\boldsymbol{b}-\boldsymbol{r}\|}, \quad (6b)$$

$$\rho_{rm} = \frac{\lambda_o}{4\pi\|\boldsymbol{r}-\boldsymbol{m}\|}. \quad (6c)$$

Finally, for a wave arriving from angle ϕ and reflected towards angle θ, the RIS radiation pattern is

$$\begin{aligned} g(\theta,\phi) &= \sqrt{G_{e,r}(\phi)G_{e,r}(\theta)}\bar{\boldsymbol{\alpha}}_r^H(\theta)\mathrm{diag}(\bar{\boldsymbol{\omega}})\bar{\boldsymbol{\alpha}}_r(\phi) \\ &= \sqrt{G_{e,r}(\phi)G_{e,r}(\theta)}N_r\boldsymbol{\alpha}_r^H(\theta)\mathrm{diag}(\boldsymbol{\omega})\boldsymbol{\alpha}_r(\phi), \end{aligned} \quad (7)$$

where $G_{e,r}(\theta)$ is the RIS element gain towards θ and $\bar{\boldsymbol{\omega}} = \mathbf{1}_{N_r} \otimes \boldsymbol{\omega} \in \mathbb{C}^{N_r^2}$ accounts for the tunable RIS response. In light of the considered two-dimensional geometry, we assume a common response along each RIS row, with $[\boldsymbol{\omega}]_n = \sqrt{G_a}\,\mathrm{e}^{\mathrm{i}\psi_n}$, where G_a is amplification gain (common to all elements) and ψ_n is the phase response of the n-th RIS element, for $n = 1,\dots,N_r$.

A. TRANSMIT SIGNAL

On each subcarrier, the BS emits Q orthogonal pilot sequences over L consecutive OFDM intervals (referred to as a frame), with $L \geq Q$. The discrete-time signal emitted on the k-th subcarrier in the ℓ-th interval is

$$\boldsymbol{s}_k[\ell] = \sqrt{L\mathcal{P}_k}\boldsymbol{F}^*\boldsymbol{p}_k[\ell] \in \mathbb{C}^{N_b}, \quad (8)$$

for $k = 1,\dots,K$ and $\ell = 1,\dots,L$, where $\boldsymbol{F} \in \mathbb{C}^{N_b\times Q}$ is a beamforming matrix normalized to have $\mathrm{tr}\{\boldsymbol{F}\boldsymbol{F}^H\} = 1$, and $\boldsymbol{p}_k[\ell] \in \mathbb{C}^Q$ is the vector of pilot symbols. Let $\boldsymbol{P}_k = [\boldsymbol{p}_k[1]\dots\boldsymbol{p}_k[L]] \in \mathbb{C}^{Q\times L}$ be the matrix containing the pilot symbols sent over a frame; we assume $\boldsymbol{P}_k\boldsymbol{P}_k^H = \boldsymbol{I}_Q$, so that $\mathcal{P}_k = \frac{1}{L}\sum_{\ell=1}^L \|\boldsymbol{s}_k[\ell]\|^2$ is the power radiated on the k-th subcarrier and $\mathcal{P}_{\mathrm{Tx}} = \sum_{k=1}^K \mathcal{P}_k$ is the total radiated power.

B. CHANNEL MODEL

Let $\rho_{brm} = \rho_{br}\rho_{rm}$ and $\tau_{brm} = \tau_{br} + \tau_{rm}$. Then, the direct and indirect channels between the BS and MS on the k-th subcarrier are

$$\begin{aligned} \boldsymbol{H}_{k,bm} &= x_{bm}\rho_{bm}\,\mathrm{e}^{-\mathrm{i}\,2\pi\,\tau_{bm}Wk} \\ &\quad\times\boldsymbol{\alpha}_m(\phi_{bm})\boldsymbol{\alpha}_b^T(\theta_{bm}) \in \mathbb{C}^{N_m\times N_b}, \end{aligned} \quad (9a)$$

$$\begin{aligned} \boldsymbol{H}_{k,brm} &= x_{brm}\rho_{brm}\,\mathrm{e}^{-\mathrm{i}\,2\pi\,\tau_{brm}Wk}\,g(\theta_{rm},\phi_{br}) \\ &\quad\times\boldsymbol{\alpha}_m(\phi_{rm})\boldsymbol{\alpha}_b^T(\theta_{br}) \in \mathbb{C}^{N_m\times N_b}, \end{aligned} \quad (9b)$$

[2] $(N_b-1)\delta_b$, $\sqrt{2}(N_r-1)\delta_r$, and $(N_m-1)\delta_m$ are the array sizes of the BS, RIS, and MS, respectively.

[3] Hereafter, angles are positive when measured anticlockwise. AODs are denoted by θ, while AOAs are denoted by ϕ.

respectively, for $k = 1, \ldots, K$. Here, $x_{bm} = e^{\mathrm{i}\,\chi_{bm}}$ and $x_{brm} = e^{\mathrm{i}\,\chi_{brm}}$ are unit-modulus complex numbers that account for the propagation phase along the direct and indirect paths, respectively, and for any synchronization error between the transmitting BS and the receiving MS.

C. RECEIVED SIGNAL

The signal received by the MS on the k-th subcarrier in the ℓ-th frame interval is

$$\tilde{\boldsymbol{y}}_k[\ell] = \big(\boldsymbol{H}_{k,bm} + \boldsymbol{H}_{k,brm}\big)\boldsymbol{s}_k[\ell] + \tilde{\boldsymbol{z}}_k[\ell] + \tilde{\boldsymbol{v}}_k[\ell] \in \mathbb{C}^{N_m}, \quad (10)$$

for $k = 1, \ldots, K$ and $\ell = 1, \ldots, L$, where $\tilde{\boldsymbol{z}}_k[\ell]$ is the noise at the MS receiver, while $\tilde{\boldsymbol{v}}_k[\ell]$ accounts for the dynamic noise at the active RIS. The entries of $\tilde{\boldsymbol{z}}_k[\ell]$ are modeled as independent complex circularly-symmetric Gaussian variables with variance σ_z^2. Moreover, following [25], [27], [28], we assume that

$$\tilde{\boldsymbol{v}}_k[\ell] = \underbrace{\rho_{rm}\bar{\boldsymbol{\alpha}}_r^T(\theta_{rm})\mathrm{diag}\{\bar{\boldsymbol{\omega}}\}\tilde{\boldsymbol{d}}_k[\ell]}_{\tilde{v}_k[\ell]}\boldsymbol{\alpha}_m(\phi_{rm}), \quad (11)$$

where the j-th entry of $\tilde{\boldsymbol{d}}_k[\ell] \in \mathbb{C}^{N_r^2}$ is the dynamic noise at the j-th RIS element on the k-th subcarrier in the ℓ-th symbol interval. The entries of $\tilde{\boldsymbol{d}}_k[\ell]$ are modeled as independent complex circularly-symmetric Gaussian variables with variance σ_d^2, so that $\tilde{v}_k[\ell]$ is a complex circularly-symmetric Gaussian with variance $\sigma_v^2 = \rho_{rm}^2\|\bar{\boldsymbol{\omega}}\|^2\sigma_d^2$. Notice that $\tilde{\boldsymbol{v}}_k[\ell]$ is proportional to the MS steering vector and its power depends upon the RIS amplification gain and the pathloss along the RIS-MS hop. The vectors $\{\tilde{\boldsymbol{z}}_k[\ell], \tilde{\boldsymbol{d}}_k[\ell]\}_{k,\ell}$ are assumed independent.

The signals received on the k-th subcarrier over a frame are organized into a matrix. Upon defining $\tilde{\boldsymbol{Y}}_k = [\tilde{\boldsymbol{y}}_k[1] \ldots \tilde{\boldsymbol{y}}_k[L]] \in \mathbb{C}^{N_m \times L}$, $\tilde{\boldsymbol{Z}}_k = [\tilde{\boldsymbol{z}}_k[1] \ldots \tilde{\boldsymbol{z}}_k[L]] \in \mathbb{C}^{N_m \times L}$, and $\tilde{\boldsymbol{V}}_k = [\tilde{\boldsymbol{v}}_k[1] \ldots \tilde{\boldsymbol{v}}_k[L]] \in \mathbb{C}^{N_m \times L}$, we have

$$\tilde{\boldsymbol{Y}}_k = \sqrt{L\mathcal{P}_k}\big(\boldsymbol{H}_{k,bm} + \boldsymbol{H}_{k,brm}\big)\boldsymbol{F}^*\boldsymbol{P}_k + \tilde{\boldsymbol{Z}}_k + \tilde{\boldsymbol{V}}_k. \quad (12)$$

Finally, after post-multiplying $\tilde{\boldsymbol{Y}}_k$ by $\boldsymbol{P}_k^H$, we obtain

$$\boldsymbol{Y}_k = \sqrt{L\mathcal{P}_k}\big(\boldsymbol{H}_{k,bm} + \boldsymbol{H}_{k,brm}\big)\boldsymbol{F}^* + \boldsymbol{Z}_k + \boldsymbol{V}_k \in \mathbb{C}^{N_m \times Q}, \quad (13)$$

where $\boldsymbol{Z}_k = \tilde{\boldsymbol{Z}}_k\boldsymbol{P}_k^H$ and $\boldsymbol{V}_k = \tilde{\boldsymbol{V}}_k\boldsymbol{P}_k^H$.

III. PROPOSED ESTIMATORS

In this section, we propose several estimators that can be employed by the MS to self-estimate its position and orientation. Following [12], [13], x_{bm} and x_{brm} are treated as unknown deterministic quantities at the design stage: indeed, errors in the estimation of the direct and indirect path lengths in the order of the carrier wavelength or larger result in hard to predict phase changes in x_{bm} and x_{brm}. At the design stage, we also consider different levels of system cognition, namely,

- Case 1: the MS has knowledge of the BS beamforming matrix $\boldsymbol{F}$, the RIS response $\boldsymbol{\omega}$, and the channel amplitudes in (6), which are shared in advance by the BS.
- Case 2: the MS has knowledge of BS beamforming matrix $\boldsymbol{F}$, while the RIS response $\boldsymbol{\omega}$ and the channel amplitudes in (6) are unknown;
- Case 3: the MS has no knowledge of the BS beamforming matrix $\boldsymbol{F}$, the RIS response $\boldsymbol{\omega}$, and the channel amplitudes in (6).

For each case, we derive the ML estimator of the MS position and orientation. For Case 1, we also derive a reduced-complexity suboptimal implementation of the ML solution, while for Case 3 we propose a reduced-complexity heuristic solution.

A. CASE 1

To proceed, we recast the signals received across all subcarriers into the vector $\boldsymbol{y} = \mathrm{vec}\{[\mathrm{vec}\{\boldsymbol{Y}_1\} \ldots \mathrm{vec}\{\boldsymbol{Y}_K\}]\} \in \mathbb{C}^{KQN_m}$. Let $\boldsymbol{x} = [x_{bm}, x_{brm}]^T$ be the vector containing the unknown channel phases along the direct and indirect links. Also, let $\boldsymbol{S} = [\boldsymbol{s}_{bm}\, \boldsymbol{s}_{brm}]$ be the matrix containing the space-frequency signatures of the signals received from the direct and indirect links, defined as

$$\boldsymbol{s}_{bm} = \rho_{bm}\boldsymbol{t}(\tau_{bm}) \otimes \boldsymbol{F}^H\boldsymbol{\alpha}_b(\theta_{bm}) \otimes \boldsymbol{\alpha}_m(\phi_{bm}), \quad (14a)$$

$$\boldsymbol{s}_{brm} = \rho_{brm}g(\theta_{rm}, \phi_{br})\boldsymbol{t}(\tau_{brm}) \otimes \boldsymbol{F}^H\boldsymbol{\alpha}_b(\theta_{br}) \otimes \boldsymbol{\alpha}_m(\phi_{rm}), \quad (14b)$$

respectively, with

$$\boldsymbol{t}(\tau) = \big[\sqrt{L\mathcal{P}_1}\,\mathrm{e}^{-\mathrm{i}\,2\pi\tau W} \;\cdots\; \sqrt{L\mathcal{P}_K}\,\mathrm{e}^{-\mathrm{i}\,2\pi\tau WK}\big]^T. \quad (15)$$

Then, we have

$$\boldsymbol{y} = \boldsymbol{S}\boldsymbol{x} + \boldsymbol{z} + \boldsymbol{v}, \quad (16)$$

where $\boldsymbol{z}$ and $\boldsymbol{v}$ are the vectorized forms of the received noise and are defined similarly to $\boldsymbol{y}$.

The following remarks are now in order. The total added noise $\boldsymbol{z} + \boldsymbol{v}$ is a complex circularly-symmetric Gaussian vector with covariance matrix $\boldsymbol{C} = \boldsymbol{I}_{KQ} \otimes \boldsymbol{\Sigma}(\phi_{rm})$, with

$$\boldsymbol{\Sigma}(\phi_{rm}) = \sigma_z^2\boldsymbol{I}_{N_m} + \sigma_v^2\boldsymbol{\alpha}_m(\phi_{rm})\boldsymbol{\alpha}_m^H(\phi_{rm}). \quad (17)$$

Also, the space-frequency signature vectors in (14) can be distinguished based on the different energy, TOFs, AODs, and AOAs along the direct and indirect links. Since the MS has knowledge of the location of the BS and RIS and is synchronized with the BS, both $\boldsymbol{S}$ and $\boldsymbol{C}$ can be uniquely computed for any given target location within the inspected region.

The likelihood function of the received signal $\boldsymbol{y}$ in (16) conditioned upon $\boldsymbol{x}$, $\boldsymbol{m}$, and φ is

$$f(\boldsymbol{y}; \boldsymbol{x}, \boldsymbol{m}, \varphi) = \frac{1}{\pi^{KQN_m}\det\{\boldsymbol{C}(\boldsymbol{m}, \varphi)\}} \times \exp\left\{-\left\|\boldsymbol{C}^{-\frac{1}{2}}(\boldsymbol{m}, \varphi)(\boldsymbol{y} - \boldsymbol{S}(\boldsymbol{m}, \varphi)\boldsymbol{x})\right\|^2\right\}, \quad (18)$$

where we have made explicit the dependence of $\boldsymbol{S}$ and $\boldsymbol{C}$ upon $\boldsymbol{m}$ and φ. After exploiting the Kronecker structure of $\boldsymbol{C}(\boldsymbol{m},\varphi)$, it can be verified that

$$\det\{\boldsymbol{C}(\boldsymbol{m},\varphi)\} = \left(\left(N_m\sigma_v^2+\sigma_z^2\right)\sigma_z^{2(N_m-1)}\right)^{KQ} \tag{19}$$

is independent of $\boldsymbol{m}$ and φ. Also, we have that

$$\boldsymbol{C}^{-1}(\boldsymbol{m},\varphi) = \boldsymbol{I}_{KQ}\otimes\boldsymbol{\Sigma}^{-1}(\phi_{rm}), \tag{20}$$

where

$$\boldsymbol{\Sigma}^{-1}(\phi_{rm}) = \frac{1}{\sigma_z^2}\left(\boldsymbol{I}_{N_m}-\frac{\sigma_v^2\boldsymbol{\alpha}_m(\phi_{rm})\boldsymbol{\alpha}_m^H(\phi_{rm})}{\sigma_z^2+N_m\sigma_v^2}\right). \tag{21}$$

Accordingly, for any $\boldsymbol{m}$ and φ the ML estimate of $\boldsymbol{x}$, is

$$\begin{aligned}\hat{\boldsymbol{x}}(\boldsymbol{m},\varphi) &= \underset{\boldsymbol{x}\in\mathcal{X}}{\operatorname{argmax}} f(\boldsymbol{y};\boldsymbol{x},\boldsymbol{m},\varphi)\\ &= \underset{\boldsymbol{x}\in\mathcal{X}}{\operatorname{argmin}}\left\|\boldsymbol{C}^{-\frac{1}{2}}(\boldsymbol{m},\varphi)(\boldsymbol{y}-\boldsymbol{S}(\boldsymbol{m},\varphi)\boldsymbol{x})\right\|^2\\ &= \underset{\boldsymbol{x}\in\mathcal{X}}{\operatorname{argmin}}\,\Re\big\{x_{bm}^*x_{brm}\kappa(\boldsymbol{m},\varphi)\\ &\qquad -x_{bm}\kappa_{bm}(\boldsymbol{m},\varphi)-x_{brm}\kappa_{brm}(\boldsymbol{m},\varphi)\big\},\end{aligned} \tag{22}$$

where $\mathcal{X}=\{\boldsymbol{x}\in\mathbb{C}^2 : |x_{bm}|=|x_{brm}|=1\}$, while

$$\begin{aligned}\kappa(\boldsymbol{m},\varphi) &= \boldsymbol{s}_{bm}^H(\boldsymbol{m},\varphi)\boldsymbol{C}^{-1}(\boldsymbol{m},\varphi)\boldsymbol{s}_{brm}(\boldsymbol{m},\varphi)\\ &= \rho_{bm}\rho_{brm}g(\theta_{rm},\phi_{br})\left(\boldsymbol{t}^H(\tau_{bm})\boldsymbol{t}(\tau_{brm})\right)\\ &\quad\times\left(\boldsymbol{\alpha}_b^H(\theta_{bm})\boldsymbol{F}\boldsymbol{F}^H\boldsymbol{\alpha}_b(\theta_{br})\right)\\ &\quad\times\left(\boldsymbol{\alpha}_m^H(\phi_{bm})\boldsymbol{\Sigma}^{-1}(\phi_{rm})\boldsymbol{\alpha}_m(\phi_{rm})\right),\end{aligned} \tag{23a}$$

$$\begin{aligned}\kappa_{bm}(\boldsymbol{m},\varphi) &= \boldsymbol{y}^H\boldsymbol{C}^{-1}(\boldsymbol{m},\varphi)\boldsymbol{s}_{bm}(\boldsymbol{m},\varphi)\\ &= \rho_{bm}\boldsymbol{y}^H\Big(\boldsymbol{t}(\tau_{bm})\otimes\boldsymbol{F}^H\boldsymbol{\alpha}_b(\theta_{bm})\\ &\quad\otimes\boldsymbol{\Sigma}^{-1}(\phi_{rm})\boldsymbol{\alpha}_m(\phi_{bm})\Big),\end{aligned} \tag{23b}$$

$$\begin{aligned}\kappa_{brm}(\boldsymbol{m},\varphi) &= \boldsymbol{y}^H\boldsymbol{C}^{-1}(\boldsymbol{m},\varphi)\boldsymbol{s}_{brm}(\boldsymbol{m},\varphi)\\ &= \rho_{brm}g(\theta_{rm},\phi_{br})\boldsymbol{y}^H\\ &\quad\times\Big(\boldsymbol{t}(\tau_{brm})\otimes\boldsymbol{F}^H\boldsymbol{\alpha}_b(\theta_{br})\\ &\quad\otimes\boldsymbol{\Sigma}^{-1}(\phi_{rm})\boldsymbol{\alpha}_m(\phi_{rm})\Big),\end{aligned} \tag{23c}$$

are the scalar products between the whitened signatures of the signals received from the direct and indirect links, between the whitened channel output and whitened signature of the signal received from the direct link, and between the whitened channel output and whitened signature of the signal received from the indirect link, respectively. Then, the ML estimates of the MS position and orientation are

$$\begin{aligned}\left[\hat{\boldsymbol{m}},\hat{\varphi}\right] &= \underset{\substack{\boldsymbol{m}\in\mathcal{M}\\ \varphi\in\Phi}}{\operatorname{argmax}} f\big(\boldsymbol{y};\hat{\boldsymbol{x}}(\boldsymbol{m},\varphi),\boldsymbol{m},\varphi\big)\\ &= \underset{\substack{\boldsymbol{m}\in\mathcal{M}\\ \varphi\in\Phi}}{\operatorname{argmin}}\left\|\boldsymbol{C}^{-\frac{1}{2}}(\boldsymbol{m},\varphi)\big(\boldsymbol{y}-\boldsymbol{S}(\boldsymbol{m},\varphi)\hat{\boldsymbol{x}}(\boldsymbol{m},\varphi)\big)\right\|^2.\end{aligned} \tag{24}$$

The computation of (22) and (24) requires a joint search over the variables $\boldsymbol{x}$, $\boldsymbol{m}$, and φ, which belong to a 5-dimensional space; upon approximating the continuous search through a discrete search, the resulting computational complexity scales quadratically with the size of the data vector and linearly with the number of grid points, i.e., it is $\mathcal{O}(E_{\boldsymbol{x},\boldsymbol{m},\varphi}(KQN_m)^2)$, wherein $E_{\boldsymbol{x},\boldsymbol{m},\varphi}$ denotes the number of points in the adopted 5-dimensional grid.

1) SUBOPTIMAL ML-BASED ESTIMATOR

If we had $\kappa(\boldsymbol{m},\varphi)=0$ for any $\boldsymbol{m}\in\mathcal{M}$ and $\varphi\in\Phi$, then Problem (22) would become

$$\hat{\boldsymbol{x}}(\boldsymbol{m},\varphi) = \underset{\boldsymbol{x}\in\mathcal{X}}{\operatorname{argmin}}\,\Re\{-x_{bm}\kappa_{bm}(\boldsymbol{m},\varphi)-x_{brm}\kappa_{brm}(\boldsymbol{m},\varphi)\}. \tag{25}$$

Remarkably, the above problem is separable over x_{bm} and x_{brm} and admits the following closed-form solution

$$\hat{x}_{bm}(\boldsymbol{m},\varphi) = \mathrm{e}^{-\mathrm{i}\angle\kappa_{bm}(\boldsymbol{m},\varphi)}, \tag{26a}$$

$$\hat{x}_{brm}(\boldsymbol{m},\varphi) = \mathrm{e}^{-\mathrm{i}\angle\kappa_{brm}(\boldsymbol{m},\varphi)}. \tag{26b}$$

It is seen from (23a) that $\kappa(\boldsymbol{m},\varphi)=0$ if the whitened signatures $\boldsymbol{C}^{-1/2}(\boldsymbol{m},\varphi)\boldsymbol{s}_{bm}(\boldsymbol{m},\varphi)$ and $\boldsymbol{C}^{-1/2}(\boldsymbol{m},\varphi)\boldsymbol{s}_{brm}(\boldsymbol{m},\varphi)$ are orthogonal. In practice, this orthogonality will not be strictly satisfied; nevertheless, (26) can still be used as an approximate solution to Problem (22) and plugged into (24) to obtain a suboptimal estimator. This approximation is accurate under the mild conditions that the signals received from the direct and indirect links have a comparable strength *and* that, for any $\boldsymbol{m}\in\mathcal{M}$ and $\varphi\in\Phi$, these signals have resolvable TOFs (so that $\boldsymbol{t}^H(\tau_{bm})\boldsymbol{t}(\tau_{brm})\simeq 0$), resolvable AODs (so that $\boldsymbol{\alpha}_b^H(\theta_{bm})\boldsymbol{F}\boldsymbol{F}^H\boldsymbol{\alpha}_b(\theta_{br})\simeq 0$), or resolvable AOAs (so that $\boldsymbol{\alpha}_m^H(\phi_{bm})\boldsymbol{\Sigma}^{-1}(\phi_{rm})\boldsymbol{\alpha}_m(\phi_{rm})\simeq 0$), which may be ensured by a suitable positioning of the RIS. Since the search variables are only $\boldsymbol{m}$ and φ, the computational complexity is reduced to $\mathcal{O}(E_{\boldsymbol{m},\varphi}(KQN_m)^2)$, where $E_{\boldsymbol{m},\varphi}$ denotes the number of points in the adopted 3-dimensional grid.

B. CASE 2

Here, the RIS response and the channel amplitudes are assumed unknown at the design stage: accordingly, ρ_{bm}, ρ_{brm}, and $g(\theta_{rm},\phi_{br})$ are treated here as unknown deterministic parameters. Upon defining

$$\underline{x}_{bm} = x_{bm}\rho_{bm}, \tag{27a}$$

$$\underline{x}_{brm} = x_{brm}\rho_{brm}g(\theta_{rm},\phi_{br}), \tag{27b}$$

and

$$\underline{\boldsymbol{s}}_{bm} = \boldsymbol{t}(\tau_{bm})\otimes\boldsymbol{F}^H\boldsymbol{\alpha}_b(\theta_{bm})\otimes\boldsymbol{\alpha}_m(\phi_{bm}), \tag{28a}$$

$$\underline{\boldsymbol{s}}_{brm} = \boldsymbol{t}(\tau_{brm})\otimes\boldsymbol{F}^H\boldsymbol{\alpha}_b(\theta_{br})\otimes\boldsymbol{\alpha}_m(\phi_{rm}), \tag{28b}$$

we rewrite the received signal in (16) as

$$\boldsymbol{y} = \underline{\boldsymbol{S}}(\boldsymbol{m},\varphi)\underline{\boldsymbol{x}}+\boldsymbol{z}+\boldsymbol{v}, \tag{29}$$

where $\underline{\boldsymbol{S}}(\boldsymbol{m},\varphi) = [\underline{\boldsymbol{s}}_{bm}(\boldsymbol{m},\varphi)\,\underline{\boldsymbol{s}}_{brm}(\boldsymbol{m},\varphi)]$ and $\underline{\boldsymbol{x}} = [\underline{x}_{bm},\,\underline{x}_{brm}]^T$. Upon comparing (16) with (29), it seen that $\boldsymbol{s}_{bm} = \rho_{bm}\underline{\boldsymbol{s}}_{bm}$ and $\boldsymbol{s}_{brm} = \rho_{brm}g(\theta_{rm},\phi_{br})\underline{\boldsymbol{s}}_{brm}$. Since the unknown quantities ρ_{bm}, ρ_{brm}, $g(\theta_{rm},\phi_{br})$ have been included into the vector $\underline{\boldsymbol{x}}$ in (29), $\underline{\boldsymbol{s}}_{bm}$ and $\underline{\boldsymbol{s}}_{brm}$ can be regarded as the normalized signatures of the signals received from the direct and indirect links; these normalized signatures are uniquely specified by the MS position and orientation and can be distinguished based on the different TOFs, AODs, and AOAs along the direct and indirect links.

The likelihood function of $\boldsymbol{y}$ conditioned upon $\underline{\boldsymbol{x}}$, $\boldsymbol{m}$, and φ is now

$$\underline{f}\big(\boldsymbol{y};\underline{\boldsymbol{x}},\boldsymbol{m},\varphi\big) = \frac{1}{\pi^{KQN_m}\det\{\boldsymbol{C}(\boldsymbol{m},\varphi)\}} \exp\left\{-\left\|\boldsymbol{C}^{-\frac{1}{2}}(\boldsymbol{m},\varphi)\big(\boldsymbol{y}-\underline{\boldsymbol{S}}(\boldsymbol{m},\varphi)\underline{\boldsymbol{x}}\big)\right\|^2\right\}. \quad (30)$$

For given $\boldsymbol{m}$ and φ, the ML estimates of $\underline{\boldsymbol{x}}$ is given by

$$\begin{aligned}\check{\underline{\boldsymbol{x}}}(\boldsymbol{m},\varphi) &= \underset{\underline{\boldsymbol{x}}\in\mathbb{C}^2}{\operatorname{argmax}}\,\underline{f}\big(\boldsymbol{y};\underline{\boldsymbol{x}},\boldsymbol{m},\varphi\big) \quad (31)\\ &= \Big(\boldsymbol{C}^{-\frac{1}{2}}(\boldsymbol{m},\varphi)\underline{\boldsymbol{S}}(\boldsymbol{m},\varphi)\Big)^{+}\boldsymbol{C}^{-\frac{1}{2}}(\boldsymbol{m},\varphi)\boldsymbol{y},\end{aligned}$$

so that the ML estimates of the MS position and orientation are

$$\begin{aligned}[\check{\boldsymbol{m}},\check{\varphi}] &= \underset{\substack{\boldsymbol{m}\in\mathcal{M}\\ \varphi\in\Phi}}{\operatorname{argmax}}\,\underline{f}\big(\boldsymbol{y};\check{\underline{\boldsymbol{x}}}(\boldsymbol{m},\varphi),\boldsymbol{m},\varphi\big)\\ &= \underset{\substack{\boldsymbol{m}\in\mathcal{M}\\ \varphi\in\Phi}}{\operatorname{argmax}}\left\|\boldsymbol{C}^{-\frac{1}{2}}(\boldsymbol{m},\varphi)\big(\boldsymbol{y}-\underline{\boldsymbol{S}}(\boldsymbol{m},\varphi)\check{\underline{\boldsymbol{x}}}(\boldsymbol{m},\varphi)\big)\right\|^2\\ &= \underset{\substack{\boldsymbol{m}\in\mathcal{R}\\ \varphi\in\Phi}}{\operatorname{argmin}}\left\|\big(\boldsymbol{I}_{KQN_m}-\underline{\boldsymbol{\Pi}}(\boldsymbol{m},\varphi)\big)\boldsymbol{C}^{-\frac{1}{2}}(\boldsymbol{m},\varphi)\boldsymbol{y}\right\|^2 \quad (32)\end{aligned}$$

where $\underline{\boldsymbol{\Pi}}(\boldsymbol{m},\varphi)$ is the orthogonal projector onto the column span of $\boldsymbol{C}^{-\frac{1}{2}}(\boldsymbol{m},\varphi)\underline{\boldsymbol{S}}(\boldsymbol{m},\varphi)$. Notice that the test statistic in (32) is the signal energy falling in the *noise subspace*, i.e., outside the column span of $\boldsymbol{C}^{-\frac{1}{2}}(\boldsymbol{m},\varphi)\underline{\boldsymbol{S}}(\boldsymbol{m},\varphi)$, when the MS is located in $\boldsymbol{m}$ and has orientation φ.

The computation of (32) again requires a joint search over the variables $\boldsymbol{m}$ and φ, which belong to a 3-dimensional space; upon approximating the continuous search with a discrete search, the resulting computational complexity scales quadratically with the size of the data vector and linearly with the number of grid points, i.e., it is $\mathcal{O}(E_{\boldsymbol{m},\varphi}(KQN_m)^2)$.

C. CASE 3

Here, the BS beamforming matrix, the RIS response, and the channel amplitudes are assumed unknown at the design stage: accordingly, ρ_{bm}, ρ_{brm}, $g(\theta_{rm},\phi_{br})$, and $\boldsymbol{F}$ are treated here as unknown deterministic parameters. To proceed, let $\boldsymbol{y}_k^{(q)}$ be the q^{th} column of $\boldsymbol{Y}_k$ in (13), corresponding to the q-th pilot sequence transmitted by the BS; also, let $\boldsymbol{y}^{(q)} = \text{vec}\{[\boldsymbol{y}_1^{(q)}\ldots\boldsymbol{y}_K^{(q)}]\} \in \mathbb{C}^{KN_m}$ and

$$\underline{\underline{x}}_{bm}^{(q)} = x_{bm}\rho_{bm}\Big[\boldsymbol{\alpha}_b^T(\theta_{bm})\boldsymbol{F}^*\Big]_q, \quad (33a)$$

$$\underline{\underline{x}}_{brm}^{(q)} = x_{brm}\rho_{brm}g(\theta_{rm},\phi_{br})\Big[\boldsymbol{\alpha}_b^T(\theta_{br})\boldsymbol{F}^*\Big]_q. \quad (33b)$$

Then we have

$$\boldsymbol{y}^{(q)} = \underline{\underline{\boldsymbol{S}}}(\boldsymbol{m},\varphi)\underline{\underline{\boldsymbol{x}}}^{(q)} + \boldsymbol{z}^{(q)} + \boldsymbol{v}^{(q)}, \quad (34)$$

where $\underline{\underline{\boldsymbol{S}}}(\boldsymbol{m},\varphi) = [\boldsymbol{t}(\tau_{bm})\otimes\boldsymbol{\alpha}_m(\phi_{bm})\;\;\boldsymbol{t}(\tau_{brm})\otimes\boldsymbol{\alpha}_m(\phi_{rm})]$ and $\underline{\underline{\boldsymbol{x}}}^{(q)} = [\underline{\underline{x}}_{bm}^{(q)}\;\;\underline{\underline{x}}_{brm}^{(q)}]^T$, while $\boldsymbol{z}^{(q)}$ and $\boldsymbol{v}^{(q)}$ are defined similarly to $\boldsymbol{y}^{(q)}$. For the q-th pilot sequence, the first and second columns of $\underline{\underline{\boldsymbol{S}}}(\boldsymbol{m},\varphi)$ can be regarded as the normalized signatures of the signals received from the direct and indirect links, respectively, while $\underline{\underline{\boldsymbol{x}}}^{(q)}$ contain all the unknown parameters, including the scalar factors $[\boldsymbol{\alpha}_b^T(\theta_{bm})\boldsymbol{F}^*]_q$ and $[\boldsymbol{\alpha}_b^T(\theta_{br})\boldsymbol{F}^*]_q$ depending upon q-th spatial precoder employed by the BS. These normalized signatures are uniquely specified by the MS position and orientation and can be distinguished based on the different TOFs and AOAs along the direct and indirect links.

The likelihood function of $\boldsymbol{y}^{(q)}$ conditioned upon $\underline{\underline{\boldsymbol{x}}}^{(q)}$, $\boldsymbol{m}$, and φ is now given by

$$\underline{\underline{f}}\Big(\boldsymbol{y}^{(q)};\underline{\underline{\boldsymbol{x}}}^{(q)},\boldsymbol{m},\varphi\Big) = \frac{1}{\pi^{KN_m}\det\Big\{\underline{\underline{\boldsymbol{C}}}^{-\frac{1}{2}}(\boldsymbol{m},\varphi)\Big\}} \exp\left\{-\left\|\underline{\underline{\boldsymbol{C}}}^{-\frac{1}{2}}(\boldsymbol{m},\varphi)\Big(\boldsymbol{y}^{(q)}-\underline{\underline{\boldsymbol{S}}}(\boldsymbol{m},\varphi)\underline{\underline{\boldsymbol{x}}}^{(q)}\Big)\right\|^2\right\}, \quad (35)$$

where $\underline{\underline{\boldsymbol{C}}}^{-\frac{1}{2}}(\boldsymbol{m},\varphi) = \boldsymbol{I}_K\otimes\boldsymbol{\Sigma}(\phi_{rm})$. For given $\boldsymbol{m}$ and φ, the ML estimate of the unknown gain vector $\underline{\underline{\boldsymbol{x}}}^{(q)}$ is available in closed form, i.e.,

$$\begin{aligned}\check{\underline{\underline{\boldsymbol{x}}}}^{(q)}(\boldsymbol{m},\varphi) &= \underset{\underline{\underline{\boldsymbol{x}}}^{(q)}\in\mathbb{C}^2}{\operatorname{argmax}}\,\underline{\underline{f}}\Big(\boldsymbol{y}^{(q)};\underline{\underline{\boldsymbol{x}}}^{(q)},\boldsymbol{m},\varphi\Big)\\ &= \Big(\underline{\underline{\boldsymbol{C}}}^{-\frac{1}{2}}(\boldsymbol{m},\varphi)\underline{\underline{\boldsymbol{S}}}(\boldsymbol{m},\varphi)\Big)^{+}\underline{\underline{\boldsymbol{C}}}^{-\frac{1}{2}}(\boldsymbol{m},\varphi)\boldsymbol{y}^{(q)}. \quad (36)\end{aligned}$$

Hence, the ML estimates of the MS position and orientation are

$$\begin{aligned}[\ddot{\boldsymbol{m}},\ddot{\varphi}] &= \underset{\substack{\boldsymbol{m}\in\mathcal{R}\\ \varphi\in\Phi}}{\operatorname{argmax}}\prod_{q=1}^{Q}\underline{\underline{f}}\Big(\boldsymbol{y}^{(q)};\underline{\underline{\boldsymbol{x}}}^{(q)}(\boldsymbol{m},\varphi),\boldsymbol{m},\varphi\Big)\\ &= \underset{\substack{\boldsymbol{m}\in\mathcal{R}\\ \varphi\in\Phi}}{\operatorname{argmin}}\sum_{q=1}^{Q}\left\|\Big(\boldsymbol{I}_{KN_m}-\underline{\underline{\boldsymbol{\Pi}}}(\boldsymbol{m},\varphi)\Big)\underline{\underline{\boldsymbol{C}}}^{-\frac{1}{2}}(\boldsymbol{m},\varphi)\boldsymbol{y}^{(q)}\right\|^2\end{aligned} \quad (37)$$

where $\underline{\underline{\boldsymbol{\Pi}}}(\boldsymbol{m},\varphi)$ is the orthogonal projector onto the column span of $\underline{\underline{\boldsymbol{C}}}^{-\frac{1}{2}}(\boldsymbol{m},\varphi)\underline{\underline{\boldsymbol{S}}}(\boldsymbol{m},\varphi)$. Again, the computation of (37) requires a joint search over the variables $\boldsymbol{m}$ and φ, and the resulting computational complexity is $\mathcal{O}(E_{\boldsymbol{m},\varphi}Q(KN_m)^2)$.

1) SUBOPTIMAL HEURISTIC ESTIMATOR

We derive here a low-complexity heuristic estimator, that first attempts to recover the AOAs ϕ_{bm} and ϕ_{rm} and the TOFs τ_{bm} and τ_{brm} and then uses this information to obtain the MS position and orientation. This procedure will only entail one-dimensional line searches, since each channel parameter is separately estimated.

To proceed, denote by $\boldsymbol{f}_q$ the q-th column of the beamforming matrix $\boldsymbol{F}$; also, assume at the design stage that

$$\boldsymbol{f}_q^H \boldsymbol{\alpha}_b(\theta_{br}) \approx 0, \quad q = 1, \ldots, Q-1, \tag{38a}$$

$$\boldsymbol{f}_Q^H \boldsymbol{\alpha}_b(\theta_{bm}) \approx 0, \quad \forall \boldsymbol{m} \in \mathcal{M}. \tag{38b}$$

Condition (38a) implies that the beamformers $[\boldsymbol{f}_1 \ldots \boldsymbol{f}_{Q-1}]$ are employed to only illuminate the region $\mathcal{M}$, while producing a negligible leakage towards the RIS. Similarly, condition (38b) implies that the beamformer $\boldsymbol{f}_Q$ is employed to only illuminate the RIS, while producing a negligible leakage towards the region $\mathcal{M}$. In practice, a proper design of $\boldsymbol{F}$ can satisfy these conditions when the AODs in the BS-MS and BS-RIS hops are sufficiently well separated (beyond the Rayleigh angular resolution of the BS array).

Now, let $[\boldsymbol{y}]_{k,q,1:N_m} \in \mathbb{C}^{N_m}$ be the vector containing the entries of the received signal $\boldsymbol{y}$ in (16) that correspond to the k^{th} subcarrier and the q^{th} transmit beam across all receive antennas.[4] Then, upon exploiting (38), we have

$$\begin{aligned}[\boldsymbol{y}]_{k,q,1:N_m} \approx\ & x_{bm}\rho_{bm}\sqrt{L\mathcal{P}_k}e^{-\mathrm{i}\,2\pi\,\tau_{bm}Wk} \\ & \times \boldsymbol{f}_q^H \boldsymbol{\alpha}_b(\theta_{bm})\boldsymbol{\alpha}_m(\phi_{bm}) \\ & + [\boldsymbol{z}]_{k,q,1\ :\ N_m} + [\boldsymbol{v}]_{k,q,1:N_m},\end{aligned} \tag{39}$$

for $q = 1, \ldots, Q-1$, and

$$\begin{aligned}[\boldsymbol{y}]_{k,Q,1\ :\ N_m} \approx\ & x_{brm}\rho_{brm}g(\theta_{rm},\phi_{br})\sqrt{L\mathcal{P}_k}e^{-\mathrm{i}\,2\pi\,\tau_{brm}Wk} \\ & \times \boldsymbol{f}_Q^H \boldsymbol{\alpha}_b(\theta_{br})\boldsymbol{\alpha}_m(\phi_{rm}) \\ & + [\boldsymbol{z}]_{k,Q,1\ :\ N_m} + [\boldsymbol{v}]_{k,Q,1\ :\ N_m},\end{aligned} \tag{40}$$

where the vectors $[\boldsymbol{z}]_{k,q,1\ :\ N_m}$ and $[\boldsymbol{v}]_{k,q,1\ :\ N_m}$ are defined similarly to $[\boldsymbol{y}]_{k,q,1\ :\ N_m}$. An estimate of ϕ_{bm} and ϕ_{rm} can now be obtained as[5]

$$\tilde{\phi}_{bm} = \underset{\phi\in\Phi_{bm}}{\operatorname{argmax}} \sum_{k=1}^{K}\sum_{q=1}^{Q-1}\left|\boldsymbol{\alpha}_m^H(\phi)[\boldsymbol{y}]_{k,q,1\ :\ N_m}\right|^2, \tag{41}$$

$$\tilde{\phi}_{rm} = \underset{\phi\in\Phi_{rm}}{\operatorname{argmax}} \sum_{k=1}^{K}\left|\boldsymbol{\alpha}_m^H(\phi)[\boldsymbol{y}]_{k,Q,1\ :\ N_m}\right|^2, \tag{42}$$

respectively, where the search sets Φ_{bm} and Φ_{brm} are tied to the prior uncertainty as to the MS position and orientation. Similarly, let $[\boldsymbol{y}]_{1\ :\ K,q,n} \in \mathbb{C}^K$ be the vector containing the entries of $\boldsymbol{y}$ that correspond to the q^{th} transmit beam and the n^{th} receive antenna across all subcarriers.[6] Then, upon exploiting (38), we have

$$\begin{aligned}[\boldsymbol{y}]_{1\ :\ K,q,n} \approx\ & x_{bm}\rho_{bm}\boldsymbol{f}_q^H\boldsymbol{\alpha}_b(\theta_{bm})[\boldsymbol{\alpha}_m(\phi_{bm})]_n\boldsymbol{t}(\tau_{bm}) \\ & + [\boldsymbol{z}]_{1\ :\ K,q,n} + [\boldsymbol{v}]_{1\ :\ K,q,n},\end{aligned} \tag{43}$$

for $q = 1, \ldots, Q-1$, and

$$\begin{aligned}[\boldsymbol{y}]_{1\ :\ K,Q,n} \approx\ & x_{brm}\rho_{brm}g(\theta_{rm},\phi_{br}) \\ & \times \boldsymbol{f}_Q^H\boldsymbol{\alpha}_b(\theta_{br})[\boldsymbol{\alpha}_m(\phi_{rm})]_n\boldsymbol{t}(\tau_{brm}) \\ & + [\boldsymbol{z}]_{1\ :\ K,Q,n} + [\boldsymbol{v}]_{1\ :\ K,Q,n},\end{aligned} \tag{44}$$

where $[\boldsymbol{z}]_{1\ :\ K,q,n}$ and $[\boldsymbol{v}]_{1\ :\ K,q,n}$ are defined similarly to $[\boldsymbol{y}]_{1\ :\ K,q,n}$. An estimate of τ_{bm} and τ_{brm} can now be obtained as

$$\tilde{\tau}_{bm} = \underset{\tau\in(d_{bm}^{\min}/c, d_{bm}^{\max}/c)}{\operatorname{argmax}} \sum_{q=1}^{Q-1}\sum_{n=1}^{N_m}\left|\boldsymbol{t}^H(\tau)[\boldsymbol{y}]_{1\ :\ K,q,n}\right|^2, \tag{45}$$

$$\tilde{\tau}_{brm} = \underset{\tau\in(d_{brm}^{\min}/c, d_{brm}^{\max}/c)}{\operatorname{argmax}} \sum_{n=1}^{N_m}\left|\boldsymbol{t}^H(\tau)[\boldsymbol{y}]_{1\ :\ K,Q,n}\right|^2, \tag{46}$$

respectively, where $d_{bm}^{\min}$ and $d_{bm}^{\max}$ are the minimum and maximum distance from the BS to any point in $\mathcal{M}$, respectively, and $d_{brm}^{\min}$ and $d_{brm}^{\max}$ are the minimum and maximum distance from the BS to the RIS to any point in $\mathcal{M}$, respectively.[7]

Finally, the MS position and orientation can be estimated as follows. The TOF estimates $\tilde{\tau}_{bm}$ and $\tilde{\tau}_{brm}$ directly translate to the distance estimates $\tilde{d}_{bm}$ and $\tilde{d}_{brm}$, respectively. When we move along an arch at distance $\tilde{d}_{bm}$ from the BS, there will be an AOD, say $\tilde{\theta}_{bm}$, that best matches the estimated RIS-MS distance $\tilde{d}_{rm} = \tilde{d}_{brm} - d_{br}$; in particular, we propose to compute $\tilde{\theta}_{bm}$ as

$$\tilde{\theta}_{bm} = \underset{\theta'\in\Theta_{bm}}{\operatorname{argmin}}\left|\tilde{d}_{rm} - d'_{rm}\right|, \tag{47}$$

where $d'_{rm} = \|\boldsymbol{r} - (\boldsymbol{b} + \tilde{d}_{bm}[\sin(\theta'),\ \cos(\theta')]^T)\|$; accordingly, an estimate of the MS position is

$$\tilde{\boldsymbol{m}} = \tilde{d}_{bm}\left[\sin\left(\tilde{\theta}_{bm}\right),\ \cos\left(\tilde{\theta}_{bm}\right)\right]^T. \tag{48}$$

Next, we can produce an estimate of the MS orientation as follows. From (5a) and (41), we have $\tilde{\varphi}_{bm} = \tilde{\theta}_{bm} + \pi - \tilde{\phi}_{bm}$, while from (5c) and (42) we have $\tilde{\varphi}_{rm} = \tilde{\theta}_{rm} + \pi/2 - \tilde{\phi}_{rm}$, where $\tilde{\theta}_{rm} = \arcsin((\tilde{m}_y - r_y)/\|\boldsymbol{r} - \tilde{\boldsymbol{m}}\|)$; accordingly, an estimate of the MS orientation is

$$\tilde{\varphi} = (\tilde{\varphi}_{bm} + \tilde{\varphi}_{rm})/2. \tag{49}$$

IV. PERFORMANCE ASSESSMENT

In this section, we assess the performance of the proposed solutions in the terms of root mean square error (RMSE) in the estimation of the MS position and orientation, also in comparison with the corresponding CRLBs [43]. The position and orientation RMSEs are defined as

$$\text{Position RMSE} = \sqrt{\mathrm{E}\left[\|\boldsymbol{m} - \boldsymbol{m}_{\text{est}}\|^2\right]}, \tag{50a}$$

$$\text{Orientation RMSE} = \sqrt{\mathrm{E}\left[(\varphi - \varphi_{\text{est}})^2\right]}, \tag{50b}$$

where $\boldsymbol{m}_{\text{est}}$ and φ_{est} are the estimated position and orientation, respectively.

[4] The corresponding entries, $(k, q, 1{:}N_m)$, in $\boldsymbol{y}$ are indexed by $[(k-1)QN_m + (q-1)N_m + n]$ for $n = 1, \ldots, N_m$.

[5] We assume that the antenna spacing at the MS, δ_m, satisfies $|\delta_m \sin(\phi)/\lambda_o| < 1/2$, $\forall\phi \in \Phi$, so that there is no spatial aliasing.

[6] The corresponding entries, $(1 : K, q, n)$, in $\boldsymbol{y}$ are indexed by $[(k-1)QN_m + (q-1)N_m + n]$ for $k = 1, \ldots, K$.

[7] We assume there that $(d_{bm}^{\max} - d_{bm}^{\min})W < c$ and $(d_{brm}^{\max} - d_{brm}^{\min})W < c$, so that there is no time aliasing.

A. POSITION AND ORIENTATION ERROR BOUNDS

For Cases 1, 2, and 3 in Sec. III, the CRLBs on the estimate of the MS position and orientation can be obtained from the likelihood functions in (18), (30), and (35), respectively. The presence of the dynamic noise of the active RIS differentiates the derivation of this bounds from those for a passive RIS [7].

Consider first Case 1. Let

$$\boldsymbol{\eta} = [\theta_{bm}, \phi_{bm}, \tau_{bm}, \rho_{bm}, \chi_{bm}, \theta_{rm}, \phi_{rm}, \tau_{rm}, \rho_{rm}, \chi_{brm}]^T \in \mathbb{R}^{10} \tag{51}$$

be the vector of unknown parameters. From [43], the FIM of $\boldsymbol{\eta}$, say $\boldsymbol{J}_{\boldsymbol{\eta}}$, is

$$[\boldsymbol{J}_{\boldsymbol{\eta}}]_{i,j} = 2\Re\left\{\frac{\partial \boldsymbol{\mu}(\boldsymbol{m},\varphi)}{\partial \eta_i}^H \boldsymbol{C}^{-1}(\boldsymbol{m},\varphi)\frac{\partial \boldsymbol{\mu}(\boldsymbol{m},\varphi)}{\partial \eta_j}\right\} + \operatorname{tr}\left\{\boldsymbol{C}^{-1}(\boldsymbol{m},\varphi)\frac{\partial \boldsymbol{C}(\boldsymbol{m},\varphi)}{\partial \eta_i}\boldsymbol{C}^{-1}(\boldsymbol{m},\varphi)\frac{\partial \boldsymbol{C}(\boldsymbol{m},\varphi)}{\partial \eta_j}\right\}, \tag{52}$$

where

$$\boldsymbol{\mu}(\boldsymbol{m},\varphi) = \mathrm{e}^{\mathrm{i}\,\chi_{bm}}\boldsymbol{s}_{bm}(\boldsymbol{m},\varphi) + \mathrm{e}^{\mathrm{i}\,\chi_{brm}}\boldsymbol{s}_{brm}(\boldsymbol{m},\varphi). \tag{53}$$

Now let $\boldsymbol{\zeta} = \boldsymbol{g}(\boldsymbol{\eta}) \in \mathbb{R}^5$ be the transformation from $\boldsymbol{\eta}$ to[8]

$$\boldsymbol{\zeta} = \left[m_x, m_y, \varphi, \chi_{bm}, \chi_{brm}\right]^T \in \mathbb{R}^5. \tag{54}$$

Upon defining the transformation $\boldsymbol{T} = \partial\boldsymbol{\eta}/\partial\boldsymbol{\zeta}$, the FIM of $\boldsymbol{\zeta}$, say $\boldsymbol{J}_{\boldsymbol{\zeta}}$, can be computed as

$$\boldsymbol{J}_{\boldsymbol{\zeta}} = \boldsymbol{T}\boldsymbol{J}_{\boldsymbol{\eta}}\boldsymbol{T}^T. \tag{55}$$

Accordingly, the positioning error bound (PEB) and the orientation error bound (OEB) are

$$\mathrm{PEB}(\boldsymbol{m},\varphi) = \sqrt{\operatorname{tr}\left\{\left[\boldsymbol{J}_{\boldsymbol{\zeta}}^{-1}\right]_{1:2,1:2}\right\}}, \tag{56a}$$

$$\mathrm{OEB}(\boldsymbol{m},\varphi) = \sqrt{\left[\boldsymbol{J}_{\boldsymbol{\zeta}}^{-1}\right]_{3,3}}, \tag{56b}$$

respectively. The expressions of $\boldsymbol{J}_{\boldsymbol{\eta}}$ and $\boldsymbol{T}$ are given in Appendix A.

As to Cases 2 and 3, the computation follows along the same lines; what changes are the definitions of $\boldsymbol{\eta}$ and $\boldsymbol{\zeta}$. In particular, for Case 2, we have

$$\boldsymbol{\eta} = \left[\theta_{bm}, \phi_{bm}, \tau_{bm}, \Re\left\{\underline{x}_{bm}\right\}, \Im\left\{\underline{x}_{bm}\right\}, \ldots \theta_{rm}, \phi_{rm}, \tau_{rm}, \Re\left\{\underline{x}_{brm}\right\}, \Im\left\{\underline{x}_{brm}\right\}\right]^T \in \mathbb{R}^{10}, \tag{57a}$$

$$\boldsymbol{\zeta} = \left[m_x, m_y, \varphi, \Re\left\{\underline{x}_{bm}\right\}, \Im\left\{\underline{x}_{bm}\right\}, \ldots \Re\left\{\underline{x}_{brm}\right\}, \Im\left\{\underline{x}_{brm}\right\}, \chi_{bm}, \chi_{brm}\right]^T \in \mathbb{R}^9, \tag{57b}$$

while for Case 3 we have

$$\boldsymbol{\eta} = \left[\theta_{bm}, \phi_{bm}, \tau_{bm}, \theta_{rm}, \phi_{rm}, \tau_{rm}, \ldots \Re\left\{\underline{x}_{bm}^{(1)}\right\}, \Im\left\{\underline{x}_{bm}^{(1)}\right\}, \Re\left\{\underline{x}_{brm}^{(1)}\right\}, \Im\left\{\underline{x}_{brm}^{(1)}\right\}, \ldots \Re\left\{\underline{x}_{bm}^{(Q)}\right\}, \Im\left\{\underline{x}_{bm}^{(Q)}\right\}, \Re\left\{\underline{x}_{brm}^{(Q)}\right\}, \Im\left\{\underline{x}_{brm}^{(Q)}\right\}\right]^T \in \mathbb{R}^{6+4Q}, \tag{58a}$$

$$\boldsymbol{\zeta} = \left[m_x, m_y, \varphi, \Re\left\{\underline{x}_{bm}^{(1)}\right\}, \Im\left\{\underline{x}_{bm}^{(1)}\right\}, \Re\left\{\underline{x}_{brm}^{(1)}\right\}, \Im\left\{\underline{x}_{brm}^{(1)}\right\}, \ldots \Re\left\{\underline{x}_{bm}^{(Q)}\right\}, \Im\left\{\underline{x}_{bm}^{(Q)}\right\}, \Re\left\{\underline{x}_{brm}^{(Q)}\right\}, \Im\left\{\underline{x}_{brm}^{(Q)}\right\}\right]^T \in \mathbb{R}^{3+4Q}. \tag{58b}$$

The details for computing the FIM of $\boldsymbol{\eta}$ and the transformation $\boldsymbol{T} = \partial\boldsymbol{\eta}/\partial\boldsymbol{\zeta}$ are provided in Appendices B and C for Cases 2 and 3, respectively.

[8] χ_{bm} and χ_{brm} are here nuisance parameters; also, there is a one-to-one mapping between $(\theta_{bm}, \phi_{bm}, \tau_{bm}, \rho_{bm}, \theta_{rm}, \phi_{rm}, \tau_{rm}, \rho_{rm})$ and (m_x, m_y, φ).

TABLE 1. Simulation parameters.

$f_o = 40$ GHz	$W_o = 120$ KHz
$\delta_b = \delta_m = \delta_r = \lambda_o/2$	$W = 70W_o = 8.4$ MHz
$\boldsymbol{b} = [0,0]^T$ m	$\boldsymbol{r} = [-11.58, 9.22]^T$ m
$\mathcal{M} = [22.5, 27.5] \times [41, 46]$ m^2	$\Phi \in [\pi/2, \pi]$ rad
$\mathcal{P}_{\mathrm{Total}} = 10$ mW	$G_a = 15$ dB
$N_m = 4$	$K = 4$
$N_b = 64$	$N_r = 1024$
$Q = 2$	$L = 3$

B. SIMULATION SETUP

We consider the system geometry in Fig. 1. We assume a noise power spectral density of 174 dBm/Hz and a noise figure of 10 dB; also, unless otherwise stated, the system parameters in Table 1 are employed. Following [20], [27], [28], the RIS element gain is modelled as $G_{e,r}(\phi) = 4\pi(\delta_r/\lambda)^2\cos(\phi)$. Different beampattern design criteria are available in the literature; in particular, the RIS phases are chosen here to maximize the array gain towards the direction θ_{rm}^o, corresponding the center of gravity, $\boldsymbol{m}_o$, of the inspected region, i.e., $\boldsymbol{\omega} = \sqrt{G_a}\mathrm{diag}(\boldsymbol{\alpha}_r^*(\theta_{rm}^o))\boldsymbol{\alpha}_r^*(\phi_{br})$. At the BS, a uniform power allocation across subcarriers is employed, i.e., $\mathcal{P}_k = \mathcal{P}_{\mathrm{Tx}}/K$; also, the beamforming matrix is chosen as $\boldsymbol{F} = [\boldsymbol{f}_1, \boldsymbol{f}_2]$, where

$$[\boldsymbol{f}_1]_n = \begin{cases} \frac{[\boldsymbol{\alpha}_b(\theta_{\mathcal{M}})]_n}{\sqrt{QN_b/2}}, n = 1, \ldots, N_b/2, \\ 0, n = N_b/2+1, \ldots, N_b, \end{cases} \tag{59a}$$

$$[\boldsymbol{f}_2]n = \frac{[\boldsymbol{\alpha}_b(\theta_{br})]_n}{\sqrt{QN_b}}, \quad n = 1, \ldots, N_b. \tag{59b}$$

Notice that only a subset of the BS antennas are employed to form the first beam; a simple phase alignment beamforming strategy is employed and the number of activated antennas should correspond to a main lobe that is large enough to uniformly illuminate the inspected region, $\mathcal{M}$. Instead, all antennas are employed to form a second sharp beam pointing towards the RIS. To illustrate this, in Fig. 2 we show the normalized amplitude beam patterns $|\boldsymbol{f}_1^H\boldsymbol{\alpha}_b(\theta)|$ and

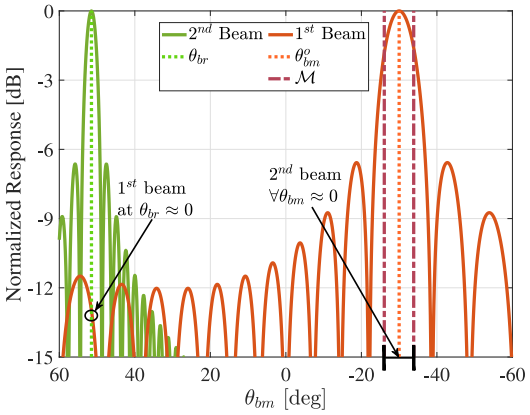

FIGURE 2. Normalized amplitude beam pattern for the first and second beam formed by the BS.

$|\boldsymbol{f}_2^H \boldsymbol{\alpha}_b(\theta)|$. It is also seen by inspection that the conditions in (38) are satisfied, i.e., the two beams are close to orthogonal.

Finally, notice that

$$\mathcal{P}_{\text{RIS}} = \mathcal{P}_{\text{Tx}} \rho_{br}^2 G_{e,r}(\phi_{br}) \left\| \boldsymbol{F}^T \boldsymbol{\alpha}_b(\theta_{br}) \right\|^2 N_r^2 (G_a - 1) \quad (60)$$

is the power radiated by the RIS. In the following we introduce a constraint on the total radiated power, i.e., $\mathcal{P}_{\text{Total}} = \mathcal{P}_{\text{Tx}} + \mathcal{P}_{\text{RIS}}$. Note that $\mathcal{P}_{\text{Total}} = \mathcal{P}_{\text{Tx}}$ when a passive RIS is considered, i.e., $G_a = 1$. When an active RIS is employed, i.e., $G_a > 1$, then $\mathcal{P}_{\text{Tx}} = \varepsilon \mathcal{P}_{\text{Total}}$ with

$$\varepsilon = \frac{1}{1 + \rho_{br}^2 G_{e,r}(\phi_{br}) \left\| \boldsymbol{F}^T \boldsymbol{\alpha}_b(\theta_{br}) \right\|^2 N_r^2 (G_a - 1)}. \quad (61)$$

Intuitively, for a fixed amplification gain, deploying the RIS closer to the BS yields a larger power radiated by the RIS: therefore the power radiated by the BS should be reduced to maintain the same $\mathcal{P}_{\text{Total}}$; similarly, for a fixed RIS location, the amplification G_a can be increased only if $\mathcal{P}_{\text{Tx}}$ is decreased. This inherent trade-off is discussed in more detail in the following examples.

For future reference, we define the received SNR as

$$\text{SNR} = (\boldsymbol{s}_{bm} + \boldsymbol{s}_{brm})^H \boldsymbol{C}^{-1} (\boldsymbol{s}_{bm} + \boldsymbol{s}_{brm}), \quad (62)$$

and the received SNR for the direct and indirect link as

$$\text{SNR}_{bm} = \boldsymbol{s}_{bm}^H \boldsymbol{C}^{-1} \boldsymbol{s}_{bm}, \quad (63a)$$
$$\text{SNR}_{brm} = \boldsymbol{s}_{brm}^H \boldsymbol{C}^{-1} \boldsymbol{s}_{brm}, \quad (63b)$$

respectively.

C. NUMERICAL EXAMPLES

Figure 3 shows the estimation performance of the proposed estimators versus $\mathcal{P}_{\text{Total}}$, also in comparison with the corresponding CRLBs. It is verified by inspection that the proposed ML estimators are asymptotically efficient, i.e., the RMSE in the estimation of the MS position and orientation converges to the corresponding CRLBs when the SNR is

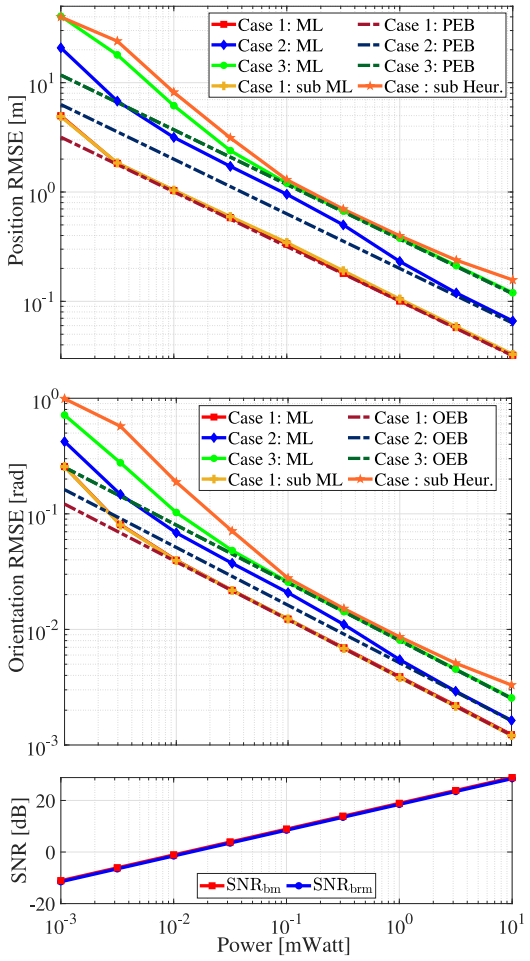

FIGURE 3. Performance of the proposed estimators versus $\mathcal{P}_{\text{Total}}$. The top and middle plots show the RMSE in the estimation of the MS position and orientation, respectively, along with the CRLBs; the bottom plot shows the received SNR for the direct and indirect links.

sufficiently large. Also, for the considered scenario, the direct and indirect links present a similar SNR. For Case 1, it is seen that the ML and suboptimal ML-based estimator provide substantially-equal performance. As expected, the estimation accuracy of the MS position and the orientation degrades in Case 2 and, even more, in Case 3, as compared to the Case 1, as a consequence of the reduced system knowledge available at the MS. Finally, in Case 3, it is interesting to notice that the proposed suboptimal heuristic estimator provides performance only slightly inferior to the ML solution for a much less implementation complexity.

Figure 4 shows the performance of the proposed estimators versus the number of subcarriers. Increasing the system bandwidth is beneficial for all solutions, as the delay resolution improves. This is more advantageous in Case 3 due to the limited system knowledge. As the system bandwidth increases, the performance gap among the ML estimators for Cases 1, 2, and 3 tends to reduce, while the performance gap between the ML and suboptimal heuristic

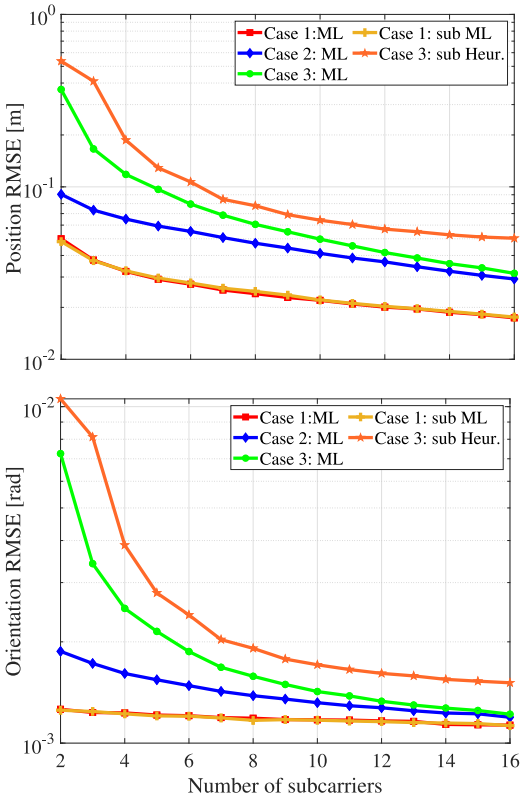

FIGURE 4. Performance of the proposed estimators versus the number of subcarriers K. The top and bottom plots show the RMSE in the estimation of the MS position and orientation, respectively.

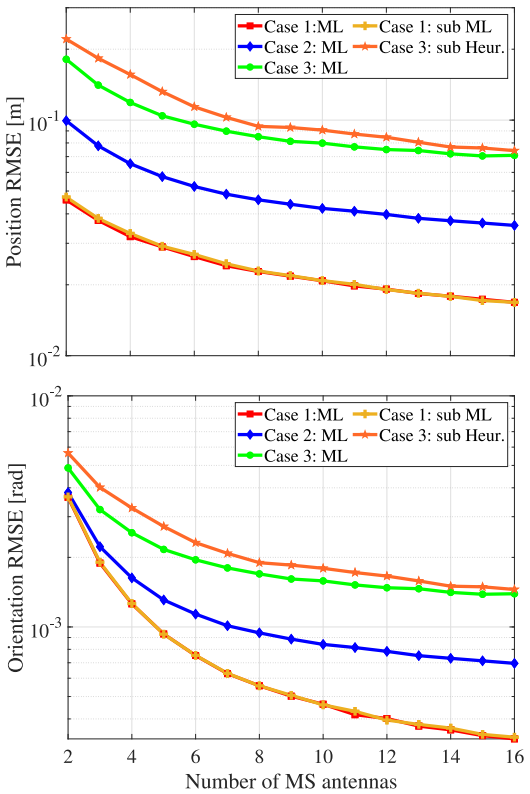

FIGURE 5. Performance of the proposed estimators versus the number of MS antenna N_m. The top and bottom plots show the RMSE in the estimation of the MS position and orientation, respectively.

estimator in Case 3 tends to increase: this phenomenon is more evident in the estimation of the MS orientation.

Figure 5 shows the performance of the proposed estimators versus the number of MS antennas. Increasing N_m is beneficial for all considered solutions, as the AOAs at the MS can be better estimated. Interestingly, this is more evident for the estimation of the MS orientation.

Figure 6 shows the performance of the proposed estimators versus the RIS amplification gain. Increasing G_a has two contrasting effects here for a fixed total radiated power. On the one hand, the power radiated by the BS is reduced, whereby the SNR on the direct link becomes smaller; on the other hand, a larger amplification gain can in principle better counteract the multiplicative pathloss in the indirect link. Accofingly, the RMSE in the estimation accuracy of the MS position and orientation of all solutions first improves as G_a starts increasing and, then, degrades. Several remarks are now in order. For a given solution, the value of G_a minimizing the RMSE in the estimation of the MS position and orientation is essentially the same. Instead, the optimal operating point is significantly different for the considered solutions. In particular, the solutions provided in Cases 2 and 3 are less robust with respect to a strong SNR imbalance between the direct and indirect links, as compared to Case 1. In addition, when there is a strong SNR imbalance between the direct and indirect links, the ML and suboptimal ML-based solutions for Case 1 diverge; a similar behaviour is also observed in Case 3, wherein the ML estimator performs much better than the suboptimal heuristic one. Finally, there is a substantial performance gain for all proposed solutions against a passive RIS ($G_a = 0$ dB) when the optimal amplification point is considered.

Figure 7 shows the performance of the proposed estimators versus the BS-RIS distance. The RIS is initially placed at the far-field limit: according to (1), the far-field limit is here 7.2 m, and this value has been marked with a dashed line. Then, the RIS is moved away from the BS along an arch which maintains a fixed distance of 50 meters with respect to the center $\boldsymbol{m}_o$ of the region $\mathcal{M}$. As the BS-RIS distance decreases, we obtain a larger SNR on the indirect link, mainly due to the fact that the pathloss along the first hop is reduced; on the other hand, the difference between the TOFs and the difference between the AOAs along the direct and indirect links reduce, thus making the corresponding received signals more correlated. The optimal RIS placement is substantially different for the considered cases. For Case 1, reducing the RIS-BS distance is always beneficial, as the prior knowledge of the signal strength on the direct and indirect links helps distinguishing these signals; instead, for Cases 2 and 3, such distance cannot be reduced too much, as the estimation of the MS position and orientation heavily relies on the TOFs and AOAs at the MS.

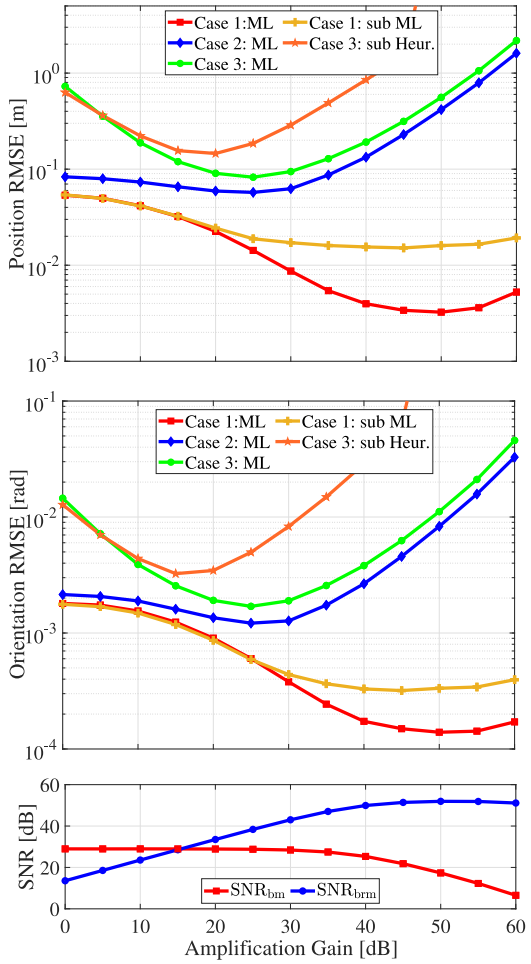

FIGURE 6. Performance of the proposed estimators versus the RIS amplification gain G_a. The top and middle plots show the RMSE in the estimation of the MS position and orientation, respectively; the bottom plot shows the received SNR for the direct and indirect links.

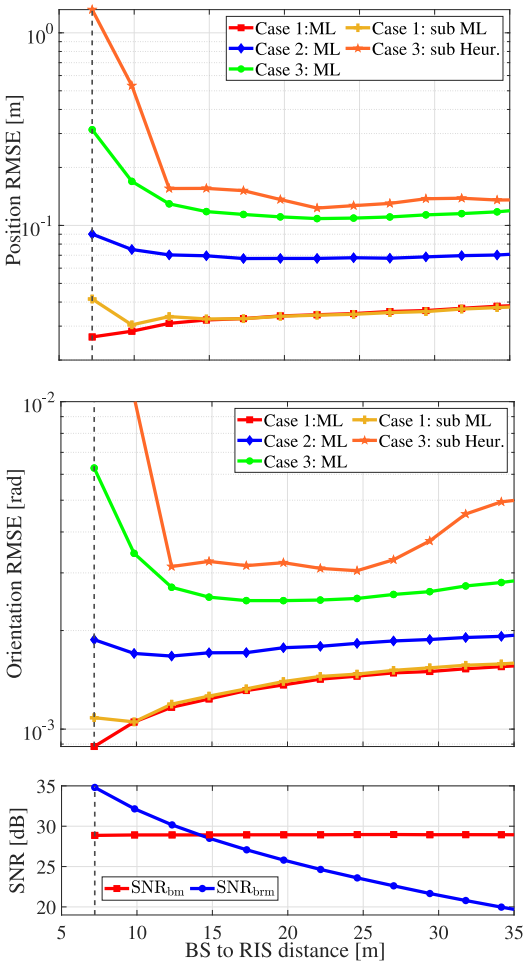

FIGURE 7. Performance of the proposed estimators versus the BS-RIS distance. The top and middle plots show the RMSE in the estimation of the MS position and orientation, respectively; the bottom plot shows the received SNR for the direct and indirect links.

To provide more insights on the impact of the RIS amplification and placement on the system performance, we finally show in Figure 8 the received SNR in (62) over a portion of the BS and RIS field of view, for different RIS placements and amplification gains. It is seen that the received SNR gets generally larger as the RIS is placed close to the BS, mainly due to the fact the pathloss along the indirect link is reduced; also, for the same BS-RIS distance, the relative strength imbalance between the direct and indirect links changes for different amplification gains. This confirm that the choice of the RIS amplification gain and placement are strictly interlaced; as discussed in Figures 6 and 7, the optimal operating point will much depend on the amount of prior system knowledge at the MS.

V. CONCLUSIONS

In this paper we have considered the problem of estimating the position and orientation of a MS based on the pilot symbols emitted by a nearby BS, which are received via both a direct link from the BS and an indirect link passing through an active RIS. After introducing a convenient signal model to account for the RIS dynamic noise, we have derived the ML estimator under three design assumptions, corresponding to a different prior knowledge of the system parameters (namely, channel amplitude, RIS response, and BS beamforming matrix) at the MS, wherein the processing is carried out. The CRLBs for each considered scenario have also been derived, which generalize previous results for passive RISs. Two low-complexity suboptimal estimators have also been proposed which take advantage of a reduced parameter search space. The provided analysis has shown that the ML solutions are asymptotically efficient and that the power amplification at the RIS can ensure that the direct and indirect links are equally reliable; in this latter case, the proposed suboptimal estimators present advantageous performance-complexity trade-offs. For a total power radiated by the BS and RIS, the RIS amplification gain and placement much affect the achievable performance. In particular, the RIS location should better guarantee a sufficient separability between the TOFs and between the AOAs along the direct and indirect links; in this regard,

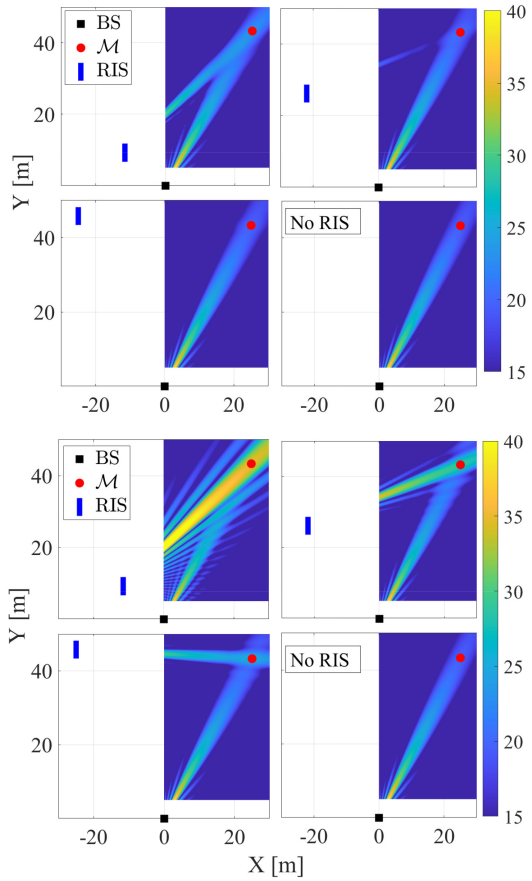

FIGURE 8. Received SNR in (62) over a portion of the BS and RIS field of view for different RIS placements and for $G_a = 15$ dB (top) and $G_a = 30$ dB (bottom)

increasing the system bandwidth and/or the number of MS antennas may also greatly help.

APPENDIX A
PARTIAL DERIVATIVES AND FIM: CASE 1

Consider the parameter vector $\boldsymbol{\eta}$ in (51); also, define

$$\boldsymbol{\mu}_{bm}(\boldsymbol{m},\varphi) = \mathrm{e}^{\mathrm{i}\,\chi_{bm}}\,\boldsymbol{s}_{bm}(\boldsymbol{m},\varphi), \tag{64a}$$

$$[\boldsymbol{\mu}_{bm}(\boldsymbol{m},\varphi)]_{k,q,n} = \sqrt{L\mathcal{P}_k}\rho_{bm}\,\mathrm{e}^{\mathrm{i}\,\chi_{bm}}\,\mathrm{e}^{-\mathrm{i}\,2\pi\,\tau_{bm}Wk} \times\Big[\boldsymbol{f}_q^H\boldsymbol{\alpha}_b(\theta_{bm})\Big]\,\mathrm{e}^{-\mathrm{i}\,2\pi\,\frac{d_b}{\lambda_o}(n-1)\sin(\phi_{bm})}, \tag{64b}$$

$$\boldsymbol{\mu}_{brm}(\boldsymbol{m},\varphi) = \mathrm{e}^{\mathrm{i}\,\chi_{brm}}\,\boldsymbol{s}_{brm}(\boldsymbol{m},\varphi), \tag{64c}$$

$$[\boldsymbol{\mu}_{brm}(\boldsymbol{m},\varphi)]_{k,q,n} = \sqrt{L\mathcal{P}_k}\rho_{brm} \times\mathrm{e}^{\mathrm{i}\,\chi_{brm}}\,g(\theta_{rm},\phi_{br})\,\mathrm{e}^{-\mathrm{i}\,2\pi\,\tau_{brm}Wk} \times\Big[\boldsymbol{f}_q^H\boldsymbol{\alpha}_b(\theta_{br})\Big]\,\mathrm{e}^{-\mathrm{i}\,2\pi\,\frac{\delta_b}{\lambda_o}(n-1)\sin(\phi_{rm})}, \tag{64d}$$

and

$$\dot{\boldsymbol{\alpha}}_b(\theta) = \frac{\partial\boldsymbol{\alpha}_b(\theta)}{\partial\theta}, \tag{65a}$$

$$\big[\dot{\boldsymbol{\alpha}}_b(\theta)\big]_n = -\,\mathrm{i}\,2\pi\,\frac{\delta_b}{\lambda_o}(n-1)\cos(\theta)\times[\boldsymbol{\alpha}_b(\theta)]_n, \tag{65b}$$

$$\dot{\boldsymbol{\alpha}}_r(\theta) = \frac{\partial\boldsymbol{\alpha}_r(\theta)}{\partial\theta}, \tag{65c}$$

$$\big[\dot{\boldsymbol{\alpha}}_r(\theta)\big]_n = -\,\mathrm{i}\,2\pi\,\frac{\delta_r}{\lambda_o}(n-1)\cos(\theta)\times[\boldsymbol{\alpha}_r(\theta)]_n, \tag{65d}$$

$$\dot{g}(\theta,\phi) = \frac{\partial g(\theta,\phi)}{\partial\theta} = N_r\pi\sqrt{\cos(\phi)} \times\left[\frac{-\sin(\theta)}{2\sqrt{\cos(\theta)}}\boldsymbol{\alpha}_r^H(\theta)\mathrm{diag}(\boldsymbol{\omega})\boldsymbol{\alpha}_r(\phi) +\sqrt{\cos(\theta)}\dot{\boldsymbol{\alpha}}_r^H(\theta)\mathrm{diag}(\boldsymbol{\omega})\boldsymbol{\alpha}_r(\phi)\right]. \tag{65e}$$

Then, we have

$$\frac{\partial[\boldsymbol{\mu}(\boldsymbol{m},\varphi)]_{k,q,n}}{\partial\theta_{bm}} = \frac{\boldsymbol{f}_q^H\dot{\boldsymbol{\alpha}}_b(\theta_{bm})}{\boldsymbol{f}_q^H\boldsymbol{\alpha}_b(\theta_{bm})}[\boldsymbol{\mu}_{bm}(\boldsymbol{m},\varphi)]_{k,q,n}, \tag{66a}$$

$$\frac{\partial[\boldsymbol{\mu}(\boldsymbol{m},\varphi)]_{k,q,n}}{\partial\phi_{bm}} = \frac{-\,\mathrm{i}\,2\pi\,\delta_m}{\lambda_o}\cos(\phi_{bm})[\boldsymbol{\mu}_{bm}(\boldsymbol{m},\varphi)]_{k,q,n}, \tag{66b}$$

$$\frac{\partial[\boldsymbol{\mu}(\boldsymbol{m},\varphi)]_{k,q,n}}{\partial\tau_{bm}} = (-\,\mathrm{i}\,2\pi\,Wk)[\boldsymbol{\mu}_{bm}(\boldsymbol{m},\varphi)]_{k,q,n}, \tag{66c}$$

$$\frac{\partial[\boldsymbol{\mu}(\boldsymbol{m},\varphi)]_{k,q,n}}{\partial\rho_{bm}} = \frac{1}{\rho_{bm}}[\boldsymbol{\mu}_{bm}(\boldsymbol{m},\varphi)]_{k,q,n}, \tag{66d}$$

$$\frac{\partial[\boldsymbol{\mu}(\boldsymbol{m},\varphi)]_{k,q,n}}{\partial\chi_{bm}} = \mathrm{i}[\boldsymbol{\mu}_{bm}(\boldsymbol{m},\varphi)]_{k,q,n}, \tag{66e}$$

$$\frac{\partial[\boldsymbol{\mu}(\boldsymbol{m},\varphi)]_{k,q,n}}{\partial\theta_{rm}} = \frac{\dot{g}(\theta_{rm},\phi_{br})}{g(\theta_{rm},\phi_{br})}[\boldsymbol{\mu}_{brm}(\boldsymbol{m},\varphi)]_{k,q,n}, \tag{66f}$$

$$\frac{\partial[\boldsymbol{\mu}(\boldsymbol{m},\varphi)]_{k,q,n}}{\partial\phi_{rm}} = \left(-\,\mathrm{i}\,2\pi\,\frac{\delta_m}{\lambda_o}\cos(\phi_{rm})\right)[\boldsymbol{\mu}_{brm}(\boldsymbol{m},\varphi)]_{k,q,n}, \tag{66g}$$

$$\frac{\partial[\boldsymbol{\mu}(\boldsymbol{m},\varphi)]_{k,q,n}}{\partial\tau_{rm}} = (-\,\mathrm{i}\,2\pi\,Wk)[\boldsymbol{\mu}_{brm}(\boldsymbol{m},\varphi)]_{k,q,n}, \tag{66h}$$

$$\frac{\partial[\boldsymbol{\mu}(\boldsymbol{m},\varphi)]_{k,q,n}}{\partial\rho_{rm}} = \frac{1}{\rho_{rm}}[\boldsymbol{\mu}_{brm}(\boldsymbol{m},\varphi)]_{k,q,n}, \tag{66i}$$

$$\frac{\partial[\boldsymbol{\mu}(\boldsymbol{m},\varphi)]_{k,q,n}}{\partial\chi_{brm}} = \mathrm{i}[\boldsymbol{\mu}_{brm}(\boldsymbol{m},\varphi)]_{k,q,n}, \tag{66j}$$

$$\frac{\partial\boldsymbol{C}}{\partial\theta_{bm}} = \frac{\partial\boldsymbol{C}}{\partial\phi_{bm}} = \frac{\partial\boldsymbol{C}}{\partial\tau_{bm}} = \frac{\partial\boldsymbol{C}}{\partial\rho_{bm}} = \frac{\partial\boldsymbol{C}}{\partial x_{bm}} = 0, \tag{66k}$$

$$\frac{\partial\boldsymbol{C}}{\partial\tau_{rm}} = \frac{\partial\boldsymbol{C}}{\partial x_{brm}} = 0, \tag{66l}$$

$$\frac{\partial\boldsymbol{C}}{\partial\theta_{rm}} = \boldsymbol{I}_{KQ}\otimes\Big(-\tan(\theta_{rm})\sigma_v^2\boldsymbol{\alpha}_m(\phi_{rm})\boldsymbol{\alpha}_m^H(\phi_{rm})\Big), \tag{66m}$$

$$\frac{\partial\boldsymbol{C}}{\partial\phi_{rm}} = \boldsymbol{I}_{KQ}\otimes\Big(\sigma_v^2\dot{\boldsymbol{a}}_m(\phi_{rm})\dot{\boldsymbol{a}}_m^H(\phi_{rm})\Big), \tag{66n}$$

$$\frac{\partial\boldsymbol{C}}{\partial\rho_{rm}} = \boldsymbol{I}_{KQ}\otimes\left(\frac{2\sigma_v^2}{\rho_{rm}}\boldsymbol{\alpha}_m(\phi_{rm})\boldsymbol{\alpha}_m^H(\phi_{rm})\right). \tag{66o}$$

The FIM of $\boldsymbol{\eta}$ is now obtained from (52). Finally, the FIM of $\boldsymbol{\zeta}$ is obtained from (55); here, the (i,j) entry of $\boldsymbol{T}$ is $[\boldsymbol{T}]_{i,j} = \partial\eta_j/\partial\zeta_i$, with $\boldsymbol{\zeta}$ given in (57b); in particular, we

have:

$$\frac{\partial\theta_{bm}}{\partial m_x}=\frac{\partial\phi_{bm}}{\partial m_x}=\frac{\frac{(b_x-m_x)^2}{d_{bm}^3}-\frac{1}{d_{bm}}}{\sqrt{1-\frac{(b_x-m_x)^2}{d_{bm}^2}}}, \tag{67a}$$

$$\frac{\partial\tau_{bm}}{\partial m_x}=\frac{-\sin(\theta_{bm})}{c}, \tag{67b}$$

$$\frac{\partial\rho_{bm}}{\partial m_x}=-\rho_{bm}\frac{m_x-b_x}{d_{bm}^2}, \tag{67c}$$

$$\frac{\partial\theta_{rm}}{\partial m_x}=\frac{\partial\phi_{rm}}{\partial m_x}=\frac{-(r_x-m_x)\big(r_y-m_y\big)}{d_{rm}^3\sqrt{1-\frac{(m_y-r_y)^2}{d_{rm}^2}}}, \tag{67d}$$

$$\frac{\partial\tau_{rm}}{\partial m_x}=\frac{\cos(\theta_{rm})}{c}, \tag{67e}$$

$$\frac{\partial\rho_{rm}}{\partial m_x}=-\rho_{rm}\frac{m_x-r_x}{d_{rm}^2}, \tag{67f}$$

$$\frac{\partial\theta_{bm}}{\partial m_y}=\frac{\partial\phi_{bm}}{\partial m_y}=\frac{\big(b_y-m_y\big)(b_x-m_x)}{d_{bm}^3\sqrt{1-\frac{(b_x-m_x)^2}{d_{bm}^2}}}, \tag{67g}$$

$$\frac{\partial\tau_{bm}}{\partial m_y}=\frac{\cos(\theta_{bm})}{c}, \tag{67h}$$

$$\frac{\partial\rho_{bm}}{\partial m_y}=-\rho_{bm}\frac{m_y-by}{d_{bm}^2}, \tag{67i}$$

$$\frac{\partial\theta_{rm}}{\partial m_y}=\frac{\partial\phi_{rm}}{\partial m_y}=\frac{\frac{-(m_y-r_y)^2}{d_{rm}^3}+\frac{1}{d_{rm}}}{\sqrt{1-\frac{(m_y-r_y)^2}{d_{rm}^2}}}, \tag{67j}$$

$$\frac{\partial\tau_{rm}}{\partial m_y}=\frac{\sin(\theta_{rm})}{c}, \tag{67k}$$

$$\frac{\partial\rho_{rm}}{\partial m_y}=-\rho_{rm}\frac{m_y-r_y}{d_{rm}^2}, \tag{67l}$$

$$\frac{\partial\theta_{bm}}{\partial\varphi}=\frac{\partial\tau_{bm}}{\partial\varphi}=\frac{\partial\rho_{bm}}{\partial\varphi}=\frac{\partial\chi_{bm}}{\partial\varphi}=0, \tag{67m}$$

$$\frac{\partial\theta_{rm}}{\partial\varphi}=\frac{\partial\tau_{rm}}{\partial\varphi}=\frac{\partial\rho_{rm}}{\partial\varphi}=\frac{\partial\chi_{brm}}{\partial\varphi}=0, \tag{67n}$$

$$\frac{\partial\phi_{bm}}{\partial\varphi}=\frac{\partial\phi_{rm}}{\partial\varphi}=-1, \tag{67o}$$

$$\frac{\partial\chi_{bm}}{\partial m_x}=\frac{\partial\chi_{bm}}{\partial m_y}=\frac{\partial\chi_{brm}}{\partial m_x}=\frac{\partial\chi_{brm}}{\partial m_y}=0, \tag{67p}$$

$$\frac{\partial\theta_{bm}}{\partial\chi_{bm}}=\frac{\partial\phi_{bm}}{\partial\chi_{bm}}=\frac{\partial\tau_{bm}}{\partial\chi_{bm}}=\frac{\partial\rho_{bm}}{\partial\chi_{bm}}=0, \tag{67q}$$

$$\frac{\partial\theta_{rm}}{\partial\chi_{bm}}=\frac{\partial\phi_{rm}}{\partial\chi_{bm}}=\frac{\partial\tau_{rm}}{\partial\chi_{bm}}=\frac{\partial\rho_{rm}}{\partial\chi_{bm}}=\frac{\partial\chi_{brm}}{\partial\chi_{bm}}=0, \tag{67r}$$

$$\frac{\partial\theta_{bm}}{\partial\chi_{brm}}=\frac{\partial\phi_{bm}}{\partial\chi_{brm}}=\frac{\partial\tau_{bm}}{\partial\chi_{brm}}=\frac{\partial\rho_{bm}}{\partial\chi_{brm}}=\frac{\partial\chi_{bm}}{\partial\chi_{brm}}=0, \tag{67s}$$

$$\frac{\partial\theta_{rm}}{\partial\chi_{brm}}=\frac{\partial\phi_{rm}}{\partial\chi_{brm}}=\frac{\partial\tau_{rm}}{\partial\chi_{brm}}=\frac{\partial\rho_{rm}}{\partial\chi_{brm}}=0, \tag{67t}$$

$$\frac{\partial\chi_{bm}}{\partial\chi_{bm}}=\frac{\partial\chi_{brm}}{\partial\chi_{brm}}=1. \tag{67u}$$

APPENDIX B
PARTIAL DERIVATIVES AND FIM: CASE 2

Consider the parameter vector $\boldsymbol{\eta}$ in (57a). The FIM of $\boldsymbol{\eta}$ is constructed similarly to Appendix A, once the quantities in (64) are replaced by

$$\boldsymbol{\mu}_{bm}(\boldsymbol{m},\varphi)=\underline{\boldsymbol{x}}_{bm}\underline{\boldsymbol{s}}_{bm}(\boldsymbol{m},\varphi), \tag{68a}$$

$$[\boldsymbol{\mu}_{bm}(\boldsymbol{m},\varphi)]_{k,q,n}=\sqrt{L\mathcal{P}_k}\underline{x}_{bm}\,\mathrm{e}^{-\mathrm{i}\,2\pi\,\tau_{bm}Wk}\times\Big[\boldsymbol{f}_q^H\boldsymbol{\alpha}_b(\theta_{bm})\Big]\mathrm{e}^{-\mathrm{i}\,2\pi\,\frac{d_b}{\lambda_o}(n-1)\sin(\phi_{bm})}, \tag{68b}$$

$$\boldsymbol{\mu}_{brm}(\boldsymbol{m},\varphi)=\underline{\boldsymbol{x}}_{brm}\underline{\boldsymbol{s}}_{brm}(\boldsymbol{m},\varphi), \tag{68c}$$

$$[\boldsymbol{\mu}_{brm}(\boldsymbol{m},\varphi)]_{k,q,n}=\sqrt{L\mathcal{P}_k}\underline{x}_{brm}\,\mathrm{e}^{-\mathrm{i}\,2\pi\,\tau_{brm}Wk}\times\Big[\boldsymbol{f}_q^H\boldsymbol{\alpha}_b(\theta_{br})\Big]\mathrm{e}^{-\mathrm{i}\,2\pi\,\frac{\delta_b}{\lambda_o}(n-1)\sin(\phi_{rm})}. \tag{68d}$$

The partial derivatives that are not found in (66) are

$$\frac{\partial[\boldsymbol{\mu}(\boldsymbol{m},\varphi)]_{k,q,n}}{\partial\Re\{\underline{x}_{bm}\}}=\frac{1}{\underline{x}_{bm}}[\boldsymbol{\mu}_{bm}(\boldsymbol{m},\varphi)]_{k,q,n}, \tag{69a}$$

$$\frac{\partial[\boldsymbol{\mu}(\boldsymbol{m},\varphi)]_{k,q,n}}{\partial\Im\{\underline{x}_{bm}\}}=\frac{\mathrm{i}}{\underline{x}_{bm}}[\boldsymbol{\mu}_{bm}(\boldsymbol{m},\varphi)]_{k,q,n}, \tag{69b}$$

$$\frac{\partial[\boldsymbol{\mu}(\boldsymbol{m},\varphi)]_{k,q,n}}{\partial\theta_{rm}}=0, \tag{69c}$$

$$\frac{\partial[\boldsymbol{\mu}(\boldsymbol{m},\varphi)]_{k,q,n}}{\partial\Re\{\underline{x}_{brm}\}}=\frac{1}{\underline{x}_{brm}}[\boldsymbol{\mu}_{brm}(\boldsymbol{m},\varphi)]_{k,q,n}, \tag{69d}$$

$$\frac{\partial[\boldsymbol{\mu}(\boldsymbol{m},\varphi)]_{k,q,n}}{\partial\Im\{\underline{x}_{brm}\}}=\frac{\mathrm{i}}{\underline{x}_{brm}}[\boldsymbol{\mu}_{brm}(\boldsymbol{m},\varphi)]_{k,q,n}. \tag{69e}$$

Note that no information can be extracted for θ_{rm}, since the RIS response is unknown. Finally, the FIM of $\boldsymbol{\zeta}$ is obtained from (55); here, the (i,j) entry of $\boldsymbol{T}$ is $[\boldsymbol{T}]_{i,j}=\partial\eta_j/\partial\zeta_i$, with $\boldsymbol{\zeta}$ given in (57b); the entries of $\boldsymbol{T}$ that are not found in (67) are

$$\frac{\partial\Re\{\underline{x}_{bm}\}}{\partial m_x}=\frac{\partial\Re\{\underline{x}_{bm}\}}{\partial m_y}=\frac{\partial\Re\{\underline{x}_{bm}\}}{\partial\varphi}=0 \tag{70a}$$

$$\frac{\partial\Re\{\underline{x}_{brm}\}}{\partial m_x}=\frac{\partial\Re\{\underline{x}_{brm}\}}{\partial m_y}=\frac{\partial\Re\{\underline{x}_{brm}\}}{\partial\varphi}=0. \tag{70b}$$

APPENDIX C
PARTIAL DERIVATIVES AND FIM: CASE 3

Consider the parameter vector $\boldsymbol{\eta}$ in (58a). The FIM of $\boldsymbol{\eta}$ is constructed similarly to Appendix A, once the quantities in (64) are replaced by

$$\boldsymbol{\mu}_{bm}(\boldsymbol{m},\varphi)=\underline{\underline{x}}_{bm}^{(q)}\boldsymbol{t}(\tau_{bm})\otimes\boldsymbol{\alpha}_m(\phi_{bm}), \tag{71a}$$

$$[\boldsymbol{\mu}_{bm}(\boldsymbol{m},\varphi)]_{k,q,n}=\sqrt{L\mathcal{P}_k}\underline{\underline{x}}_{bm}^{(q)}\times\mathrm{e}^{-\mathrm{i}\,2\pi\,\tau_{bm}Wk}\,\mathrm{e}^{-\mathrm{i}\,2\pi\,\frac{d_b}{\lambda_o}(n-1)\sin(\phi_{bm})}, \tag{71b}$$

$$\boldsymbol{\mu}_{brm}(\boldsymbol{m},\varphi)=\underline{\underline{x}}_{brm}^{(q)}\boldsymbol{t}(\tau_{brm})\otimes\boldsymbol{\alpha}_m(\phi_{rm}), \tag{71c}$$

$$[\boldsymbol{\mu}_{brm}(\boldsymbol{m},\varphi)]_{k,q,n} = \sqrt{L\mathcal{P}_k}\underline{\underline{x}}_{brm}^{(q)} \times \mathrm{e}^{-\mathrm{i}\,2\pi\,\tau_{brm}Wk}\,\mathrm{e}^{-\mathrm{i}\,2\pi\,\frac{\delta_b}{\lambda_o}(n-1)\sin(\phi_{rm})}. \tag{71d}$$

The partial derivatives that are not found in (66), are

$$\frac{\partial[\boldsymbol{\mu}(\boldsymbol{m},\varphi)]_{k,q,n}}{\partial\theta_{bm}} = 0, \tag{72a}$$

$$\frac{\partial[\boldsymbol{\mu}(\boldsymbol{m},\varphi)]_{k,q,n}}{\partial\Re\left\{\underline{\underline{x}}_{bm}^{(q)}\right\}} = \frac{1}{\underline{\underline{x}}_{bm}^{(q)}}[\boldsymbol{\mu}_{bm}(\boldsymbol{m},\varphi)]_{k,q,n}, \tag{72b}$$

$$\frac{\partial[\boldsymbol{\mu}(\boldsymbol{m},\varphi)]_{k,q,n}}{\partial\Im\left\{\underline{\underline{x}}_{bm}^{(q)}\right\}} = \frac{\mathrm{i}}{\underline{\underline{x}}_{bm}^{(q)}}[\boldsymbol{\mu}_{bm}(\boldsymbol{m},\varphi)]_{k,q,n}, \tag{72c}$$

$$\frac{\partial[\boldsymbol{\mu}(\boldsymbol{m},\varphi)]_{k,q,n}}{\partial\theta_{rm}} = 0, \tag{72d}$$

$$\frac{\partial[\boldsymbol{\mu}(\boldsymbol{m},\varphi)]_{k,q,n}}{\partial\Re\left\{\underline{\underline{x}}_{brm}^{(q)}\right\}} = \frac{1}{\underline{\underline{x}}_{brm}^{(q)}}[\boldsymbol{\mu}_{brm}(\boldsymbol{m},\varphi)]_{k,q,n}, \tag{72e}$$

$$\frac{\partial[\boldsymbol{\mu}(\boldsymbol{m},\varphi)]_{k,q,n}}{\partial\Im\left\{\underline{\underline{x}}_{brm}^{(q)}\right\}} = \frac{\mathrm{i}}{\underline{\underline{x}}_{brm}^{(q)}}[\boldsymbol{\mu}_{brm}(\boldsymbol{m},\varphi)]_{k,q,n}. \tag{72f}$$

Note that no information can be extracted for θ_{bm} and θ_{rm}, since the beamforming matrix and the RIS response are unknown. Finally, the FIM of $\boldsymbol{\zeta}$ is obtained from (55); here, the (i,j) entry of $\boldsymbol{T}$ is $[\boldsymbol{T}]_{i,j} = \partial\eta_j/\partial\zeta_i$, with $\boldsymbol{\zeta}$ given in (58b); the entries of $\boldsymbol{T}$ that are not found in (67) are

$$\frac{\partial\Re\left\{\underline{\underline{x}}_{bm}^{(q)}\right\}}{\partial m_x} = \frac{\partial\Re\left\{\underline{\underline{x}}_{bm}^{(q)}\right\}}{\partial m_y} = \frac{\partial\Re\left\{\underline{\underline{x}}_{bm}^{(q)}\right\}}{\partial\varphi} = 0, \tag{73a}$$

$$\frac{\partial\Re\left\{\underline{\underline{x}}_{brm}^{(q)}\right\}}{\partial m_x} = \frac{\partial\Re\left\{\underline{\underline{x}}_{brm}^{(q)}\right\}}{\partial m_y} = \frac{\partial\Re\left\{\underline{\underline{x}}_{brm}^{(q)}\right\}}{\partial\varphi} = 0, \tag{73b}$$

for $q = 1,\ldots,Q$.

REFERENCES

[1] E. Basar, M. Di Renzo, J. De Rosny, M. Debbah, M.-S. Alouini, and R. Zhang, "Wireless communications through reconfigurable intelligent surfaces," *IEEE Access*, vol. 7, pp. 116753–116773, 2019.

[2] E. Björnson, H. Wymeersch, B. Matthiesen, P. Popovski, L. Sanguinetti, and E. De Carvalho, "Reconfigurable intelligent surfaces: A signal processing perspective with wireless applications," *IEEE Signal Process. Mag.*, vol. 39, no. 2, pp. 135–158, Mar. 2022.

[3] S. Buzzi, C. D'Andrea, A. Zappone, M. Fresia, Y.-P. Zhang, and S. Feng, "RIS configuration, beamformer design, and power control in single-cell and multi-cell wireless networks," *IEEE Trans. Cogn. Commun.*, vol. 7, no. 2, pp. 398–411, Jun. 2021.

[4] Q. Li, M. Wen, E. Basar, G. C. Alexandropoulos, K. J. Kim, and H. V. Poor, "Channel estimation and multipath diversity reception for RIS-empowered broadband wireless systems based on cyclic-prefixed single-carrier transmission," *IEEE Trans. Wireless Commun.*, vol. 22, no. 8, pp. 5145–5156, Aug. 2023.

[5] J. Wang, S. Gong, Q. Wu, and S. Ma, "RIS-aided MIMO systems with hardware impairments: Robust beamforming design and analysis," *IEEE Trans. Wireless Commun.*, vol. 22, no. 10, pp. 6914–6929, Oct. 2023.

[6] H. Wymeersch, J. He, B. Denis, A. Clemente, and M. Juntti, "Radio localization and mapping with reconfigurable intelligent surfaces: Challenges, opportunities, and research directions," *IEEE Veh. Technol. Mag.*, vol. 15, no. 4, pp. 52–61, Dec. 2020.

[7] A. Elzanaty, A. Guerra, F. Guidi, and M.-S. Alouini, "Reconfigurable intelligent surfaces for localization: Position and orientation error bounds," *IEEE Trans. Signal Process.*, vol. 69, pp. 5386–5402, Aug. 2021.

[8] T. Ma, Y. Xiao, X. Lei, W. Xiong, and Y. Ding, "Indoor localization with reconfigurable intelligent surface," *IEEE Commun. Lett.*, vol. 25, no. 1, pp. 161–165, Jan. 2021.

[9] C. L. Nguyen, O. Georgiou, G. Gradoni, and M. Di Renzo, "Wireless fingerprinting localization in smart environments using reconfigurable intelligent surfaces," *IEEE Access*, vol. 9, pp. 135526–135541, 2021.

[10] H. Zhang, H. Zhang, B. Di, K. Bian, Z. Han, and L. Song, "Metalocalization: Reconfigurable intelligent surface aided multi-user wireless indoor localization," *IEEE Trans. Wireless Commun.*, vol. 20, no. 12, pp. 7743–7757, Dec. 2021.

[11] Y. Liu, E. Liu, R. Wang, and Y. Geng, "Reconfigurable intelligent surface aided wireless localization," in *Proc. IEEE Int. Conf. Commun. (ICC)*, 2021, pp. 1–6.

[12] A. Fascista, A. Coluccia, H. Wymeersch, and G. Seco-Granados, "RIS-aided joint localization and synchronization with a single-antenna mmWave receiver," in *Proc. IEEE Int. Conf. Acoust., Speech Signal Process. (ICASSP)*, 2021, pp. 4455–4459.

[13] K. Keykhosravi, M. F. Keskin, G. Seco-Granados, and H. Wymeersch, "SISO RIS-enabled joint 3D downlink localization and synchronization," in *Proc. IEEE Int. Conf. Commun. (ICC)*, 2021, pp. 1–6.

[14] J. He, H. Wymeersch, L. Kong, O. Silvén, and M. Juntti, "Large intelligent surface for positioning in Millimeter wave MIMO systems," in *Proc. IEEE 91st Veh. Technol. Conf. (VTC)*, 2020, pp. 1–5.

[15] D. Dardari, N. Decarli, A. Guerra, and F. Guidi, "localization in NLOS conditions using large reconfigurable intelligent surfaces," in *Proc. IEEE 22nd Int. Workshop Signal Process. Adv. Wireless Commun. (SPAWC)*, 2021, pp. 551–555.

[16] A. Parchekani and S. Valaee, "Sensing and localization using reconfigurable intelligent surfaces and the Swendsen-wang algorithm," in *Proc. IEEE Int. Conf. Commun. Workshops (ICC)*, 2022, pp. 981–986.

[17] E. Čišija, A. M. Ahmed, A. Sezgin, and H. Wymeersch, "RIS-aided mmWave MIMO radar system for adaptive multi-target localization," in *Proc. IEEE Stat. Signal Process. Workshop (SSP)*, 2021, pp. 196–200.

[18] K. Meng, Q. Wu, R. Schober, and W. Chen, "Intelligent reflecting surface enabled multi-target sensing," *IEEE Trans. Commun.*, vol. 70, no. 12, pp. 8313–8330, Dec. 2022.

[19] S. Buzzi, E. Grossi, M. Lops, and L. Venturino, "Radar target detection aided by reconfigurable intelligent surfaces," *IEEE Signal Process. Lett.*, vol. 28, pp. 1315–1319, Jun. 2021.

[20] S. Buzzi, E. Grossi, M. Lops, and L. Venturino, "Foundations of MIMO radar detection aided by reconfigurable intelligent surfaces," *IEEE Trans. Signal Process.*, vol. 70, pp. 1749–1763, Mar. 2022.

[21] K. Meng, Q. Wu, W. Chen, and D. Li, "Sensing-assisted communication in vehicular networks with intelligent surface," *IEEE Trans. Veh. Technol.*, vol. 73, no. 1, pp. 876–893, Jan. 2024.

[22] D. Dardari, N. Decarli, A. Guerra, and F. Guidi, "LOS/NLOS near-field localization with a large reconfigurable intelligent surface," *IEEE Trans. Wireless Commun.*, vol. 21, no. 6, pp. 4282–4294, Jun. 2022.

[23] Z. Abu-Shaban, K. Keykhosravi, M. F. Keskin, G. C. Alexandropoulos, G. Seco-Granados, and H. Wymeersch, "Near-field localization with a reconfigurable intelligent surface acting as lens," in *Proc. IEEE Int. Conf. Commun. (ICC)*, 2021, pp. 1–6.

[24] W. Tang et al., "Wireless communications with reconfigurable intelligent surface: Path loss modeling and experimental measurement," *IEEE Trans. Wireless Commun.*, vol. 20, no. 1, pp. 421–439, Jan. 2021.

[25] R. Long, Y.-C. Liang, Y. Pei, and E. G. Larsson, "Active reconfigurable intelligent surface-aided wireless communications," *IEEE Trans. Wireless Commun.*, vol. 20, no. 8, pp. 4962–4975, Aug. 2021.

[26] Z. Zhang et al., "Active RIS vs. passive RIS: Which will prevail in 6G?" *IEEE Trans. Commun.*, vol. 71, no. 3, pp. 1707–1725, Mar. 2023.

[27] M. Rihan, E. Grossi, L. Venturino, and S. Buzzi, "Spatial diversity in radar detection via active reconfigurable intelligent surfaces," *IEEE Signal Process. Lett.*, vol. 29, pp. 1242–1246, May 2022.

[28] E. Grossi, H. Taremizadeh, and L. Venturino, "Radar target detection and localization aided by an active reconfigurable intelligent surface," *IEEE Signal Process. Lett.*, vol. 30, pp. 903–907, Jul. 2023.

[29] M. Rihan, A. Zappone, S. Buzzi, G. Fodor, and M. Debbah, "Passive vs. active reconfigurable intelligent surfaces for integrated sensing and communication: Challenges and opportunities," *IEEE Netw.*, vol. 38, no. 3, pp. 218–226, May 2024.
[30] Z. Zhang, T. Jiang, and W. Yu, "localization with reconfigurable intelligent surface: An active sensing approach," *IEEE Trans. Wireless Commun.*, vol. 23, no. 7, pp. 7698–7711, Jul. 2024.
[31] J. Lončar, A. Grbic, and S. Hrabar, "Ultrathin active polarization-selective metasurface at X-band frequencies," *Phys. Rev. B, Condens. Matter*, vol. 100, no. 7, 2019, Art. no. 75131.
[32] K. K. Kishor and S. V. Hum, "An amplifying reconfigurable reflectarray antenna," *IEEE Trans. Antennas Propag.*, vol. 60, no. 1, pp. 197–205, Jan. 2012.
[33] J.-F. Bousquet, S. Magierowski, and G. G. Messier, "A 4-GHz active scatterer in 130-nm CMOS for phase sweep amplify-and-forward," *IEEE Trans. Circuits Syst. I, Reg. Papers*, vol. 59, no. 3, pp. 529–540, Mar. 2012.
[34] S. Taravati and G. V. Eleftheriades, "Full-duplex reflective beamsteering metasurface featuring magnetless nonreciprocal amplification," *Nat. Commun.*, vol. 12, no. 1, pp. 1–11, 2021.
[35] N. T. Nguyen, Q.-D. Vu, K. Lee, and M. Juntti, "Hybrid relay-reflecting intelligent surface-assisted wireless communications," *IEEE Trans. Veh. Technol.*, vol. 71, no. 6, pp. 6228–6244, Jun. 2022.
[36] G. C. Alexandropoulos and E. Vlachos, "A hardware architecture for reconfigurable intelligent surfaces with minimal active elements for explicit channel estimation," in *Proc. IEEE Int. Conf. Acoust., Speech Signal Process. (ICASSP)*, 2020, pp. 9175–9179.
[37] M. Hua, Q. Wu, W. Chen, Z. Fei, H. C. So, and C. Yuen, "Intelligent reflecting surface-assisted localization: Performance analysis and algorithm design," *IEEE Wireless Commun. Lett.*, vol. 13, no. 1, pp. 84–88, Jan. 2024.
[38] X. Shao, C. You, W. Ma, X. Chen, and R. Zhang, "Target sensing with intelligent reflecting surface: Architecture and performance," *IEEE J. Sel. Areas Commun.*, vol. 40, no. 7, pp. 2070–2084, Jul. 2022.
[39] G. Mylonopoulos, C. D'Andrea, and S. Buzzi, "Active reconfigurable intelligent surfaces for user localization in mmWave MIMO systems," in *Proc. IEEE 23rd Int. Workshop Signal Process. Adv. Wireless Commun. (SPAWC)*, 2022, pp. 1–5.
[40] G. Mylonopoulos, L. Venturino, S. Buzzi, and C. D'Andrea, "Maximum-likelihood user localization in active-RIS empowered mmWave wireless networks," in *Proc. 17th Eur. Conf. Antennas Propagat. (EUCAP)*, 2023, pp. 1–5.
[41] X. Shao, Q. Jiang, and R. Zhang, "6D movable antenna based on user distribution: Modeling and optimization," 2024, *arXiv:2403.08123*.
[42] W. L. Stutzman and G. A. Thiele, *Antenna Theory and Design*, 3rd ed. New York, NY, USA: Wiley, 1998.
[43] S. M. Kay, *Fundamentals of Statistical Signal Processing: Estimation Theory*. Hoboken, NJ, USA: Prentice Hall, 1997.

GEORGIOS MYLONOPOULOS (Student Member, IEEE) received the M.Sc. degree in electrical and computer engineering from the Aristotle University of Thessaloniki in 2021. He is currently pursuing the Ph.D. degree with the University of Cassino and Southern Lazio, Italy. Since 2021, he is an Early-Stage Researcher for the EU funded Innovative Training Network Project METAWIRELESS, on the application of metasurfaces to wireless communications. His research interests are in broad area of signal processing for localization, detection, and sensing in wireless communication applications.

LUCA VENTURINO (Senior Member, IEEE) received the Ph.D. degree in electrical engineering from the University of Cassino and Southern Lazio, Italy, in 2006. From 2006–2008, he had a short-term visiting appointments with the Mobile and Signal Processing Department, NEC Laboratories America, Princeton, NJ, USA. In 2004, 2009, 2022, and 2024, he had short-term visiting appointments with the Electrical Engineering Department, Columbia University, New York, USA. From 2011 to 2017, he was an external consultant for the Space and Avionic Division of Leonardo (formerly, Selex ES and Selex Galileo), Nerviano, Italy. Since 2006, he has been with the Department of Electrical and Information Engineering, University of Cassino and Southern Lazio, where he is currently a Full Professor of Telecommunications and the Chair of the Quality Assurance Committee. His research interests are in broad area of signal processing for detection, estimation, and resource allocation in wireless communication and radar applications. He currently serves as a Senior Area Editor for the IEEE TRANSACTIONS ON SIGNAL PROCESSING; formerly, he served as a Senior Area Editor for the IEEE SIGNAL PROCESSING LETTERS and an Associate Editor for the IEEE TRANSACTIONS ON SIGNAL PROCESSING and the IEEE SIGNAL PROCESSING LETTERS.

STEFANO BUZZI (Senior Member, IEEE) received the M.Sc. degree (summa cum laude) in electronic engineering and the Ph.D. degree in electrical and computer engineering from the University of Naples "Federico II" in 1994 and 1999, respectively. He had short-term research appointments with Princeton University, Princeton, NJ, USA, in 1999, 2000, 2001, and 2006. He joined the University of Cassino and Southern Lazio, Italy, in 2000, where he was an Assistant Professor and has been an Associate Professor since 2002 and a Full Professor since 2018. He is the General Coordinator of the EU Funded Innovative Training Network Project METAWIRELESS, on the application of metasurfaces to wireless communications, and the EU-Funded Doctoral Network ISLANDS, on integrated sensing and communications for the vehicular environment. He has coauthored about 180 technical peer-reviewed journals and conference papers, and, among these, the highly cited paper "What will 5G be?," IEEE JOURNAL ON SELECTED AREAS IN COMMUNICATIONS, in June 2014. His current research interests include communications and signal processing, with an emphasis on wireless communications and beyond-5G systems. He serves regularly as a TPC member for several international conferences. He is a former Associate Editor of IEEE SIGNAL PROCESSING LETTERS and IEEE COMMUNICATIONS LETTERS and has been the Guest Editor of four IEEE JOURNAL ON SELECTED AREAS IN COMMUNICATIONS special issues. From 2014 to 2020, he was an Editor of IEEE TRANSACTIONS ON WIRELESS COMMUNICATIONS. He is currently an Associate Editor of IEEE TRANSACTIONS ON COMMUNICATIONS.

CARMEN D'ANDREA (Member, IEEE) received the B.S., M.S., and Ph.D. degrees (summa cum laude) in telecommunications engineering from the University of Cassino and Southern Lazio, Italy, in 2013, 2015, and 2019 respectively, where she is currently a non-tenured Assistant Professor. In 2017, she was a visiting Ph.D. student with the Wireless Communications (WiCom) Research Group, Department of Information and Communication Technologies, Universitat Pompeu Fabra, Barcelona, Spain. In the spring of 2020, she spent three months as a Visiting Researcher with the Communication System Division, Department of Electrical Engineering, Linkoping University, Sweden. In June 2023, she received the Best Paper Award at EUCNC and 6G Summit 2023. In 2023, she received the Italian Scientific Habilitation (ASN) as an Associate Professor; she is in the World's Top 2% Scientists 2023 in the topic "Information & Communication Technologies - Networking & Telecommunications" listed by Elsevier, Scopus, and Standford University and in the list of "100 Brilliant and Inspiring Women in 6G" List for 2024. Her research interests focus on wireless communication and signal processing, with emphasis on mmWave communications, massive MIMO systems, and the study of waveforms for beyond-5G communication systems. Since 2020, she has been an Associate Editor for IEEE COMMUNICATIONS LETTERS (Exemplary Editor in 2022) and IEEE OPEN JOURNAL OF THE COMMUNICATIONS SOCIETY.

Open Access funding provided by 'Università degli Studi di Cassino e del Lazio Meridionale' within the CRUI CARE Agreement